

Rotation Curves of Spiral Galaxies: I

Rotation of spiral nebulae was first noticed by Wolf and by Slipher in 1914. Pease (1916, 1918) made first measurements of what we now call the “rotation curve” in the nuclear regions of M31 and M104 (“Sombrero”).

Before ~1975 it was believed that after reaching maximum the rotation velocity

History: goes down as $V \sim R^{-1/2}$. Mass of a galaxy was taken as (Brandt’s 1960 model):

$$M_{\text{tot}} = (3/2)^{3/n} V_{\text{max}}^2 R_{\text{max}} / G,$$

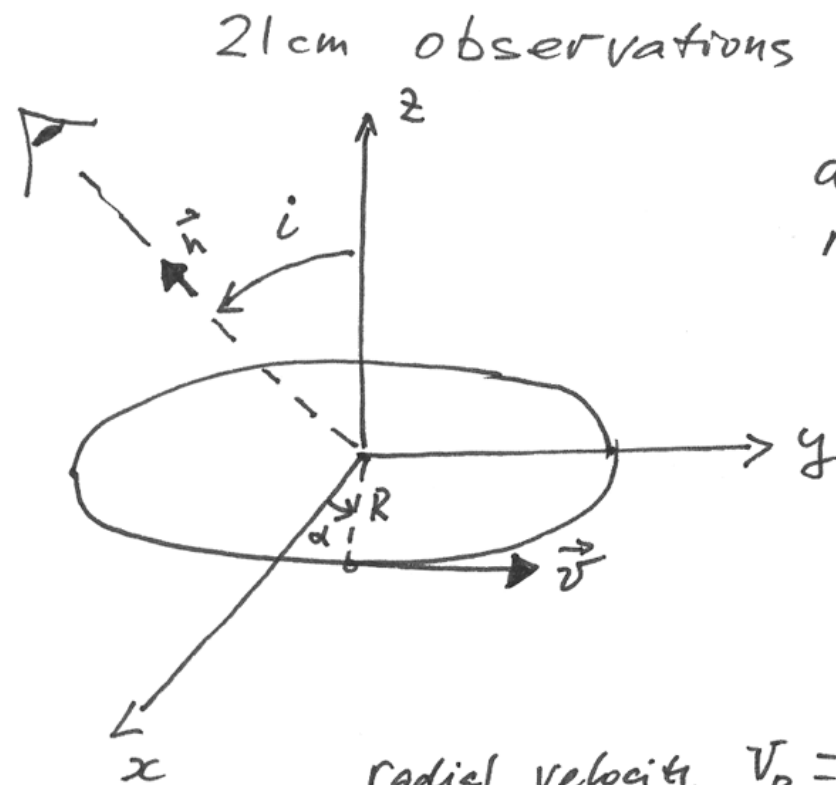
where n is a parameter in the following approximation for the rotation curve:

$$V_{\text{rot}} = V_{\text{max}} (R/R_{\text{max}}) / [1/3 + 2/3 * (R/R_{\text{max}})^n]^{3/2n}$$

The situation changed around 1975 when 21cm measurements showed that the velocity V_{rot} does not decline beyond optical radius. Rubin, Ford, and Thonnard (1978) pushed optical observations to larger radii with the same basic conclusion as in 21cm: flat rotation curves. For review of early results see Faber & Gallagher (1979, ARAAS 17). F&G gave for spiral galaxies within the Holmberg radius (26.5mag/arcsec):

$$(M/L)_B \approx (M/L)_V \approx 5 \text{ for Sb spirals. } (M/L) \text{ decreases for later types.}$$

Recovering rotation curves using 21cm observations



assume that V is a function of radius R :

$$V = \omega(R) R$$

$$\vec{n} = \{0, -\sin i, \cos i\}$$

$$\vec{v} = \{-V \sin i, V \cos i, 0\}$$

$$\text{radial velocity } V_R = -V \sin i \cos \alpha = -\frac{V}{R} \sin i \cdot x$$

→ get $\sin i$ from axial ratio of the galaxy (a/b)

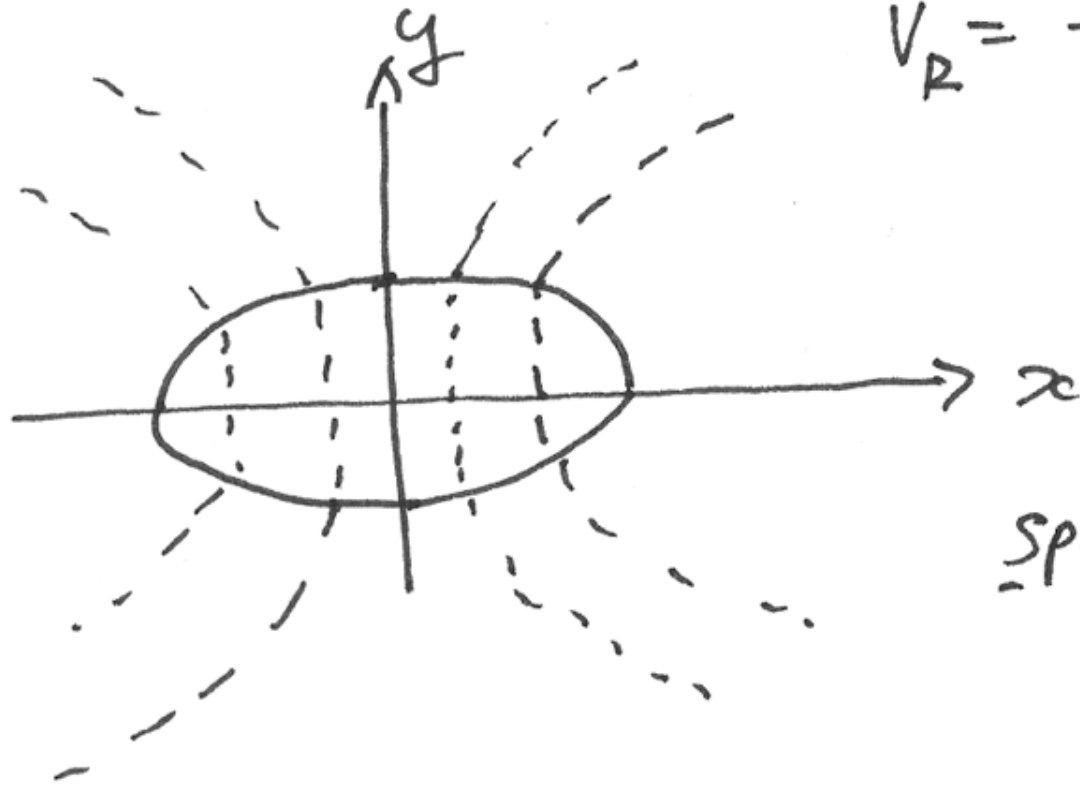
→ V_R - measured

Two limiting cases:

1) solid-body rotation: $V_R = -\frac{V}{R} \cdot \sin i \cdot x =$
 $= \text{constant along } x$

2) flat rotation:

$$V_R = - (V \sin i) \frac{x}{\sqrt{x^2 + y^2}}$$



spider diagram

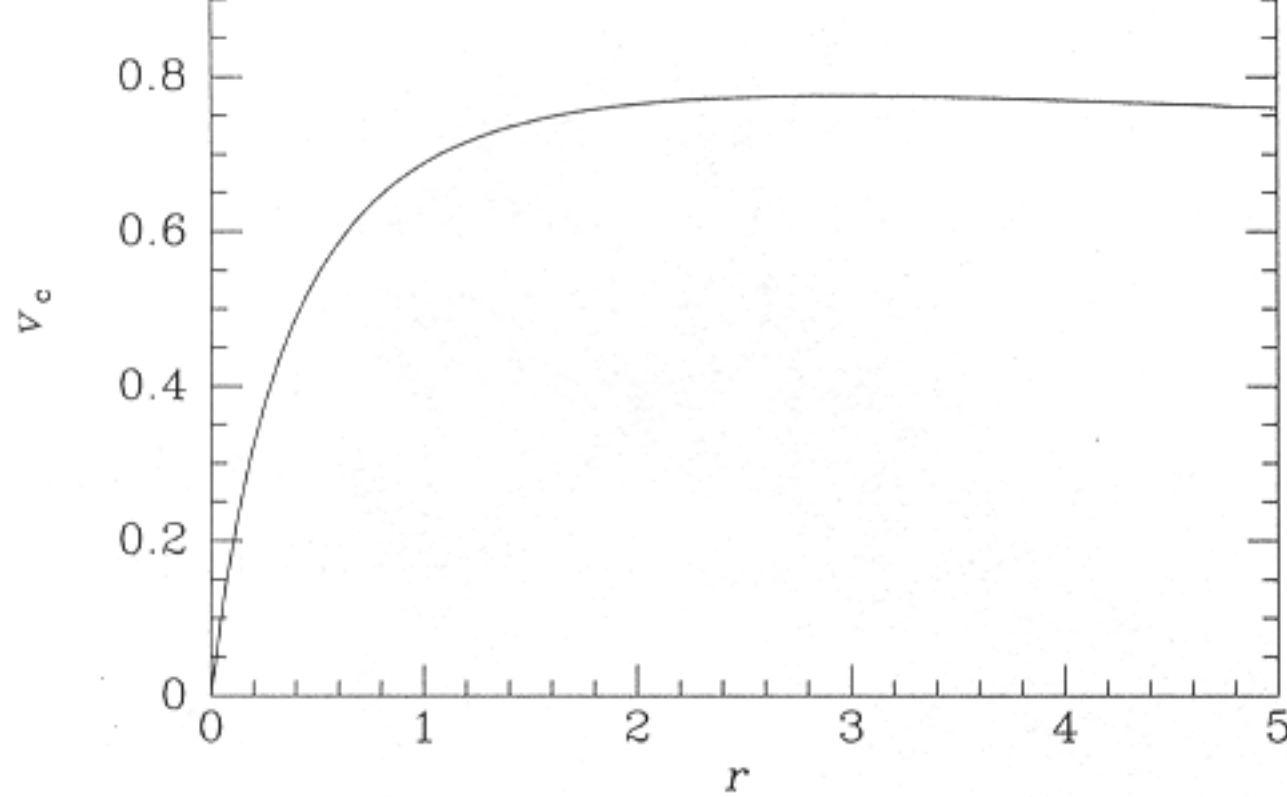


Figure 8.31 A typical galactic circular-speed curve.

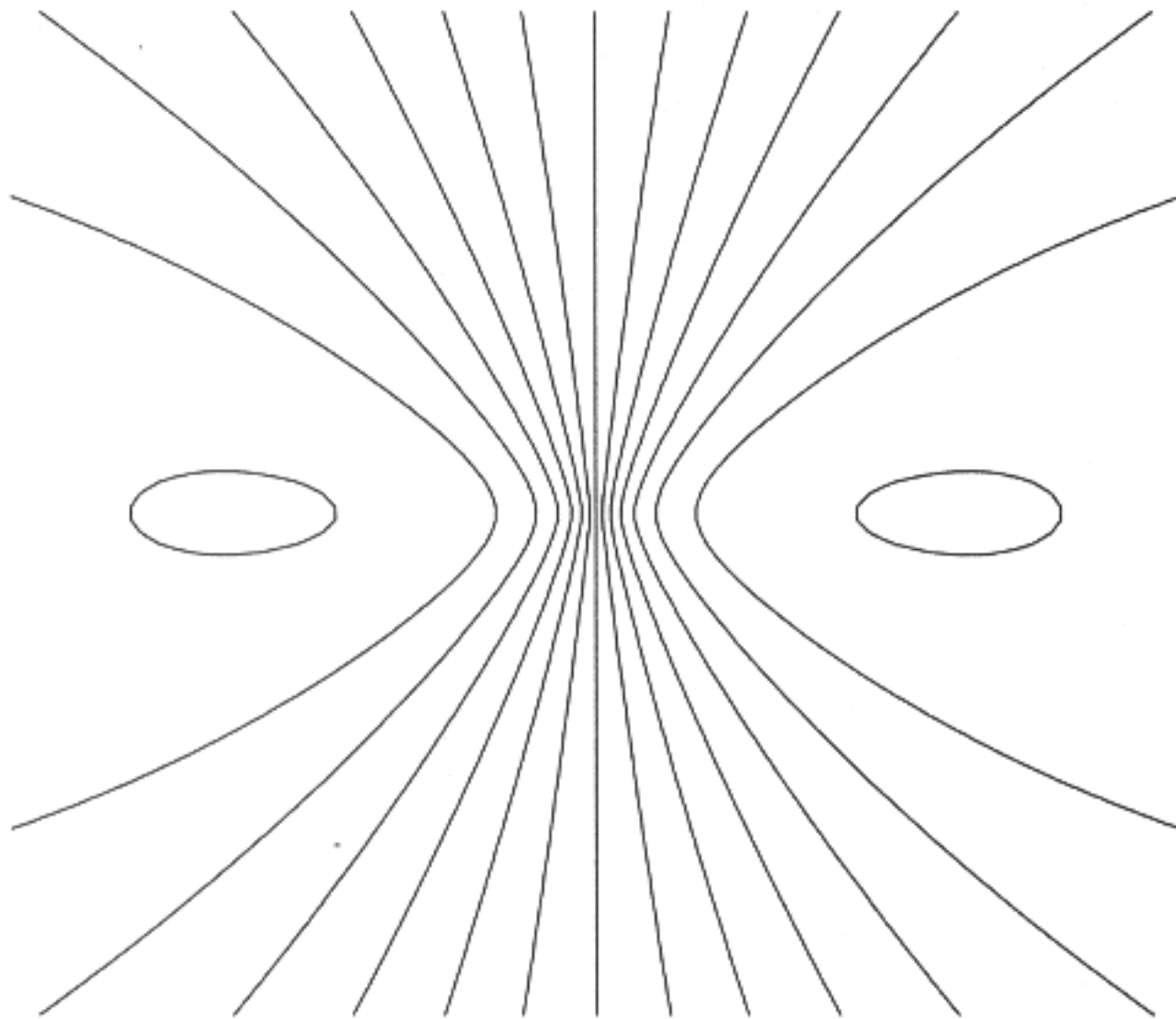


Figure 8.32 The spider diagram generated by the circular-speed curve of Figure 8.31 when the system is viewed at inclination $i = 30^\circ$ with the apparent major axis horizontal. The area contoured is a square 10 distance units on a side.

Complications:
oval distortions.

The galaxy is
clearly barred

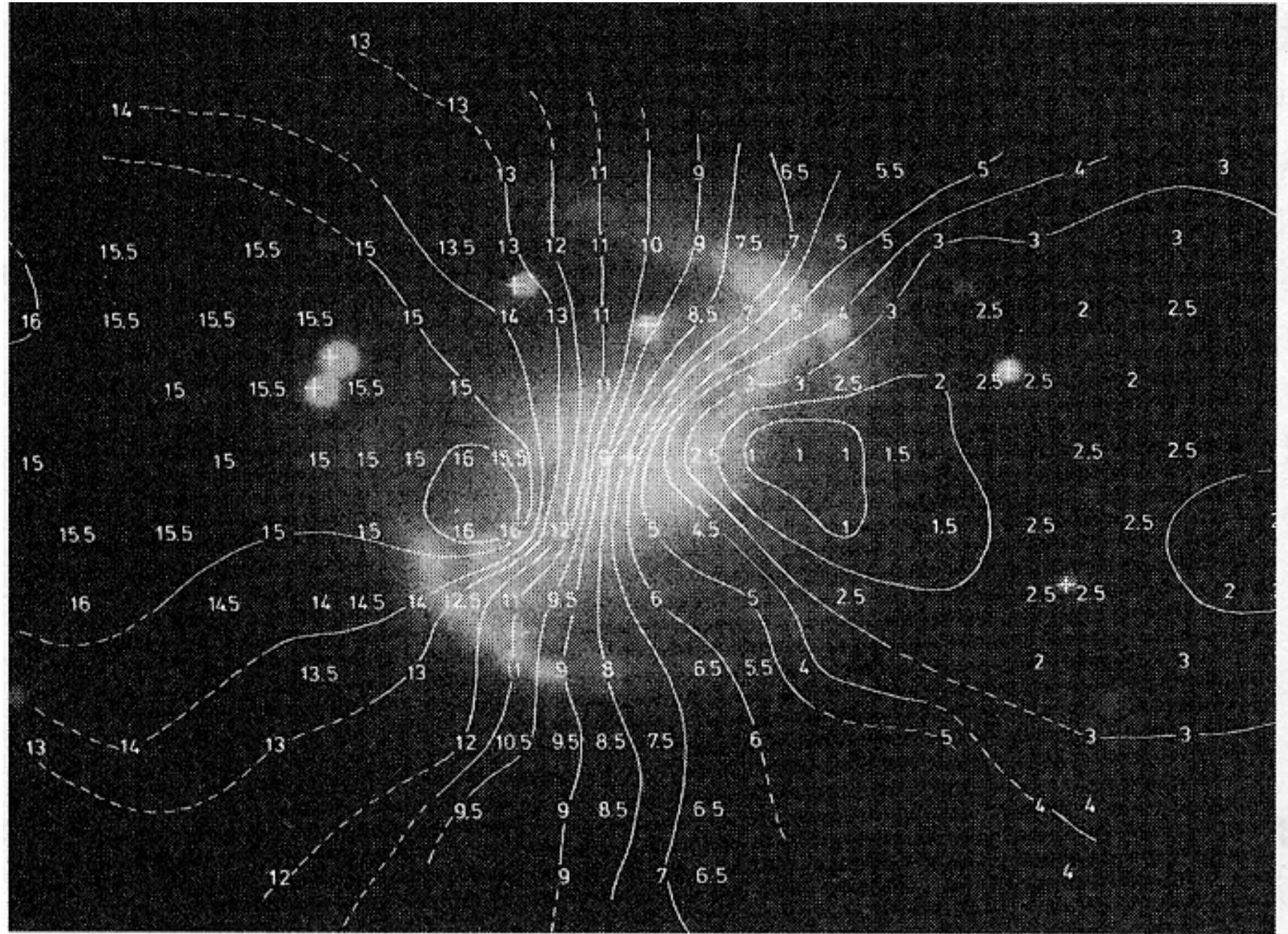


Figure 8.39 The HI constant-velocity contours of NGC 5383 superimposed on an optical image of the galaxy. The spider diagram is approximately twofold symmetric, but the kinematic major and minor axes are by no means perpendicular. This is the signature of an elliptical disk. [After Sancisi, Allen & Sullivan (1979) courtesy of R. Sancisi]

Tilted ring model:
pure circular motion
inside each ring, but
rings are tilted.

Note that the spider
diagram is twisted.

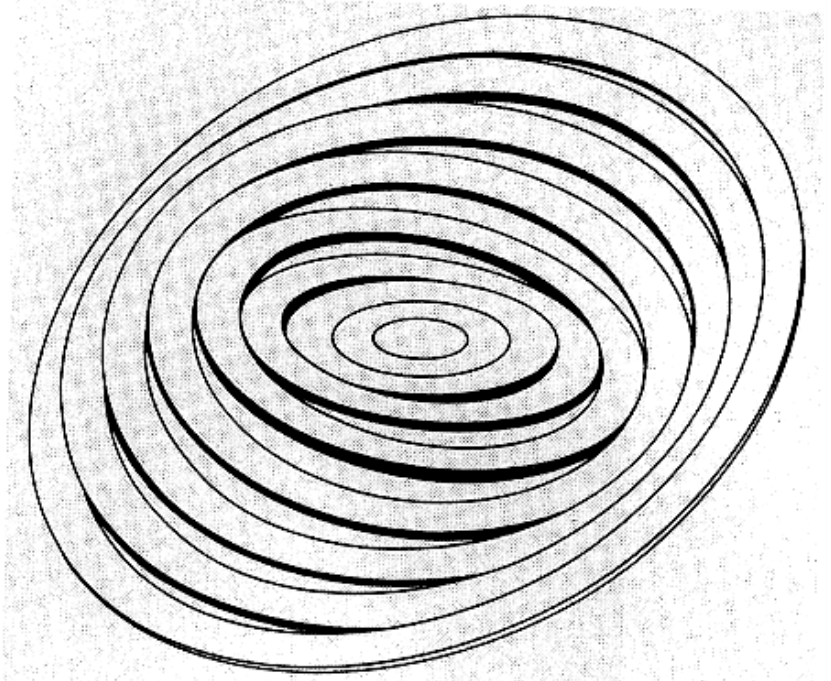
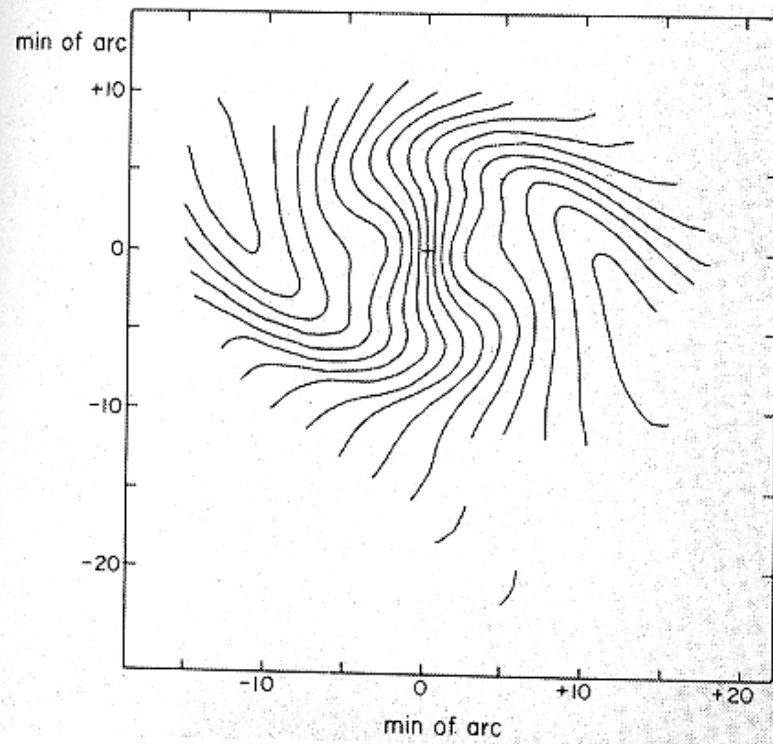


Figure 8.36 A tilted ring model of M83 (right) and the spider diagram predicted by this model (left). [After Rogstad, Lockhart & Wright (1974)]

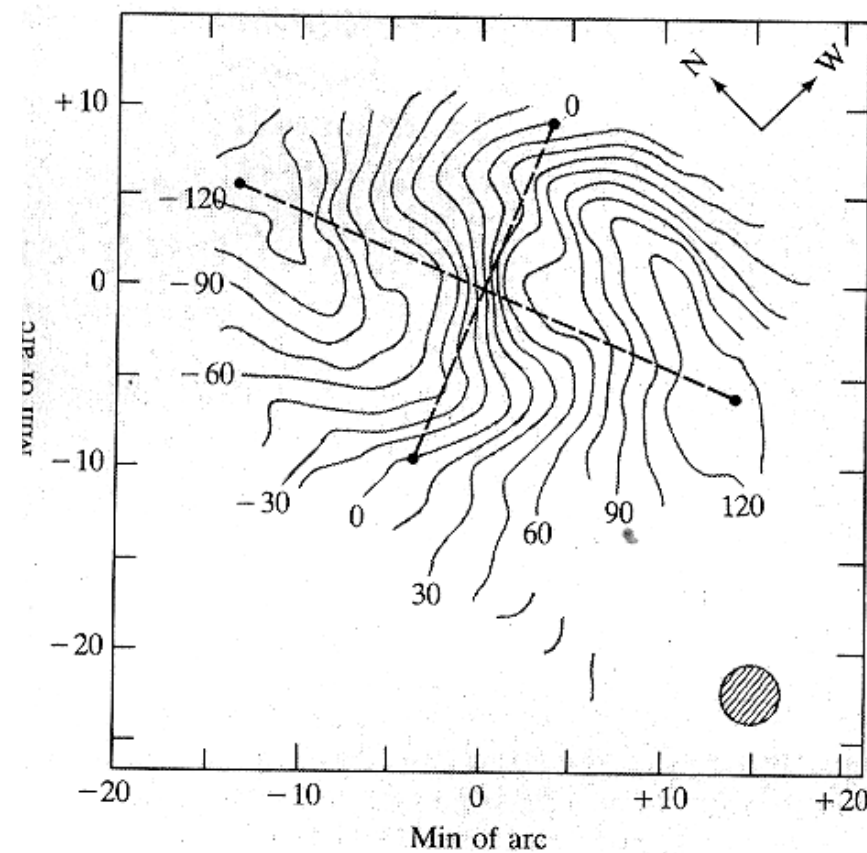


Figure 8.37 The observed spider diagram of M83. [After Rogstad, Lockhart & Wright (1974)]

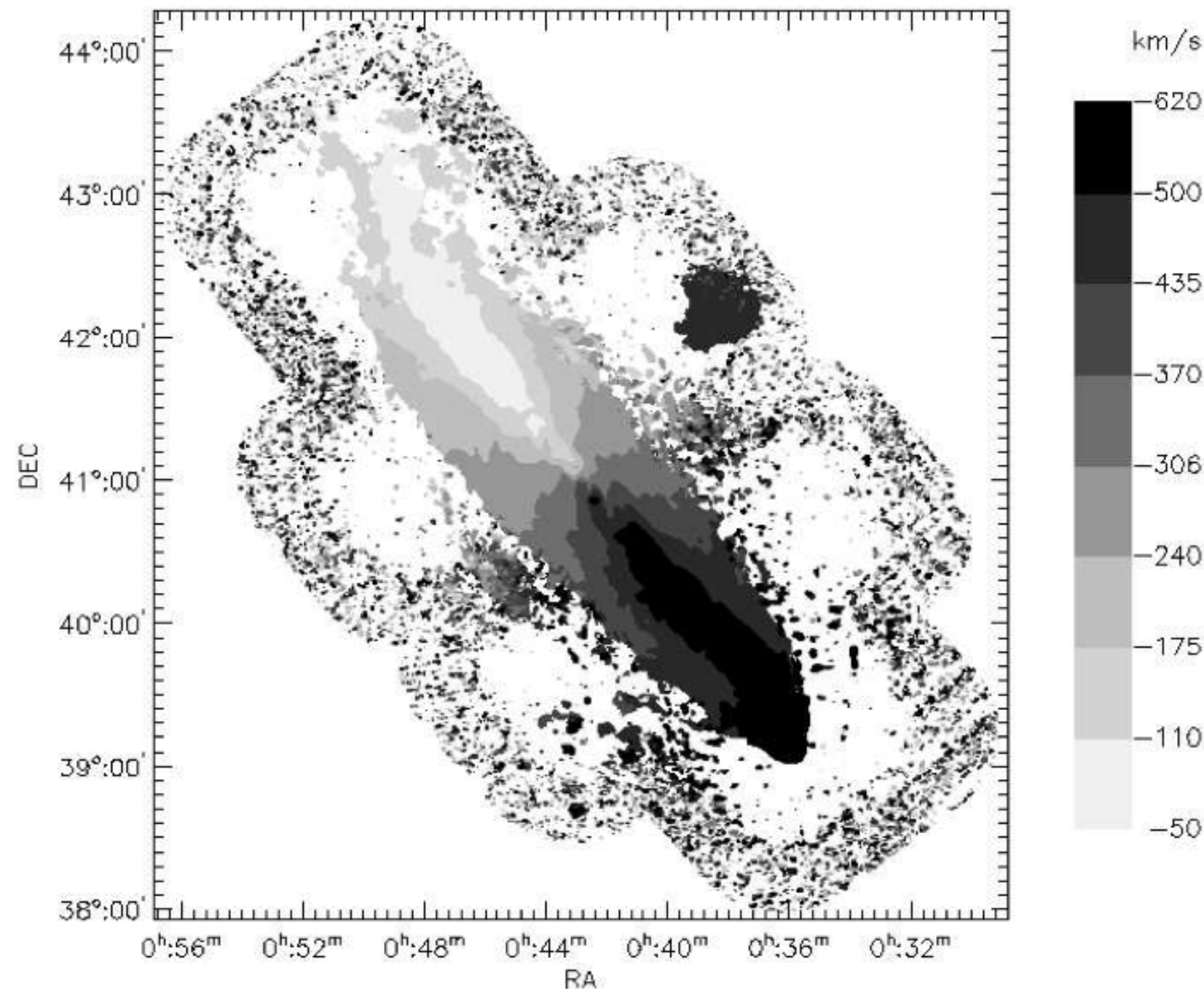


Fig. 1. The first moment map. The intensity-weighted mean velocity has been computed from the 120 arcsec data cube at a spectral resolution of 2 km s^{-1} , using a $4\text{-}\sigma$ blanking in the data cube at 18.5 km/s resolution to determine what is included in the integral.

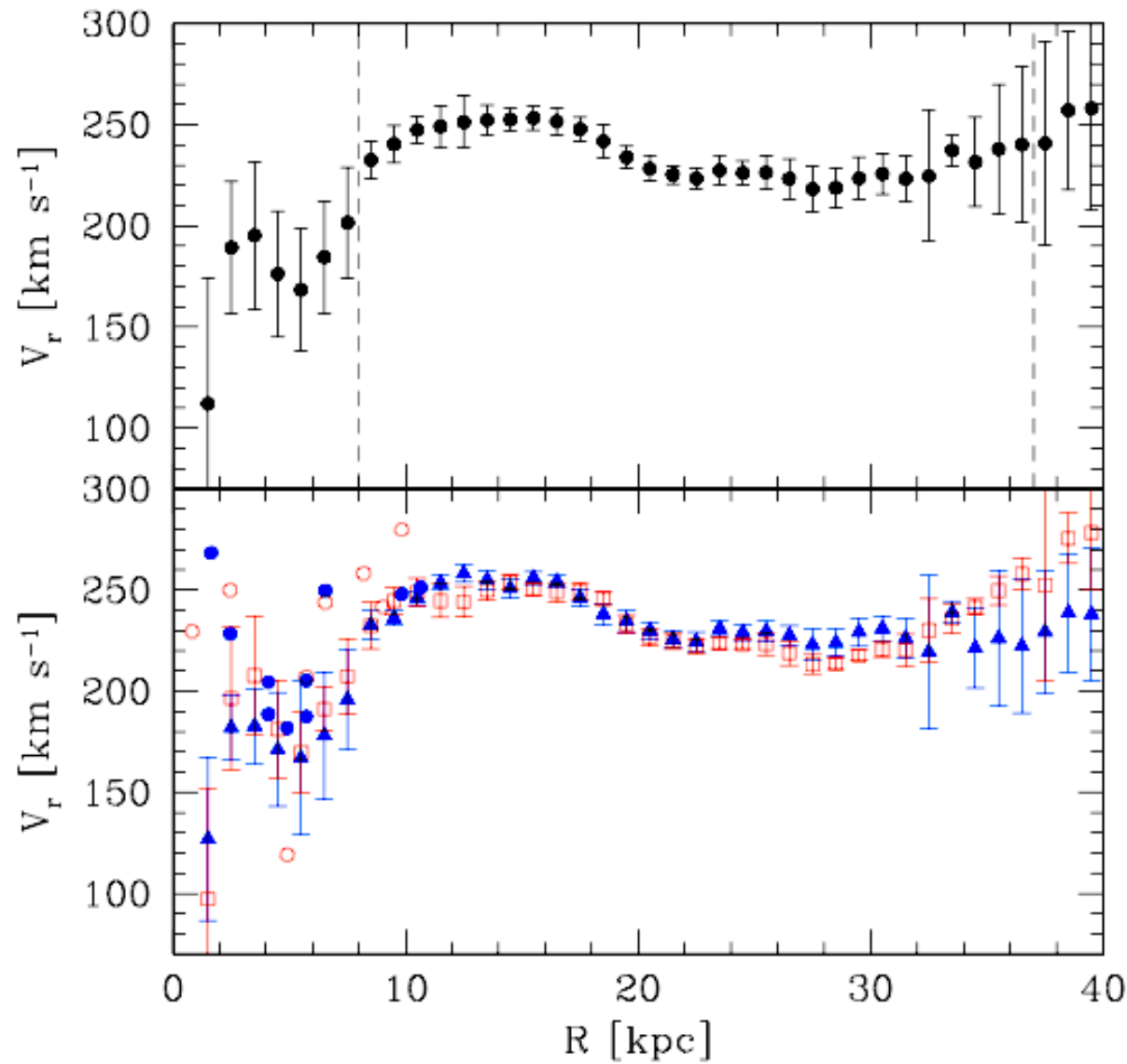


Fig. 7. The bottom panel shows the rotation curves obtained for the northern and southern halves of the galaxy by averaging the data shown in Fig. 6 in radial bins 1 kpc wide. Errorbars refer to the dispersion around the mean. Filled triangles are for the northern half, open squares for the southern half of the galaxy. Rotational velocities in the inner region derived from CO data by Loinard et al. (1995) are shown with filled and open circles for the northern and southern major axis, assumed to be at PA = 38° and with $i = 77^\circ$. The filled dots in the upper panel show the global rotation curve. As explained in the text, errorbars

Corbelli et al 2010

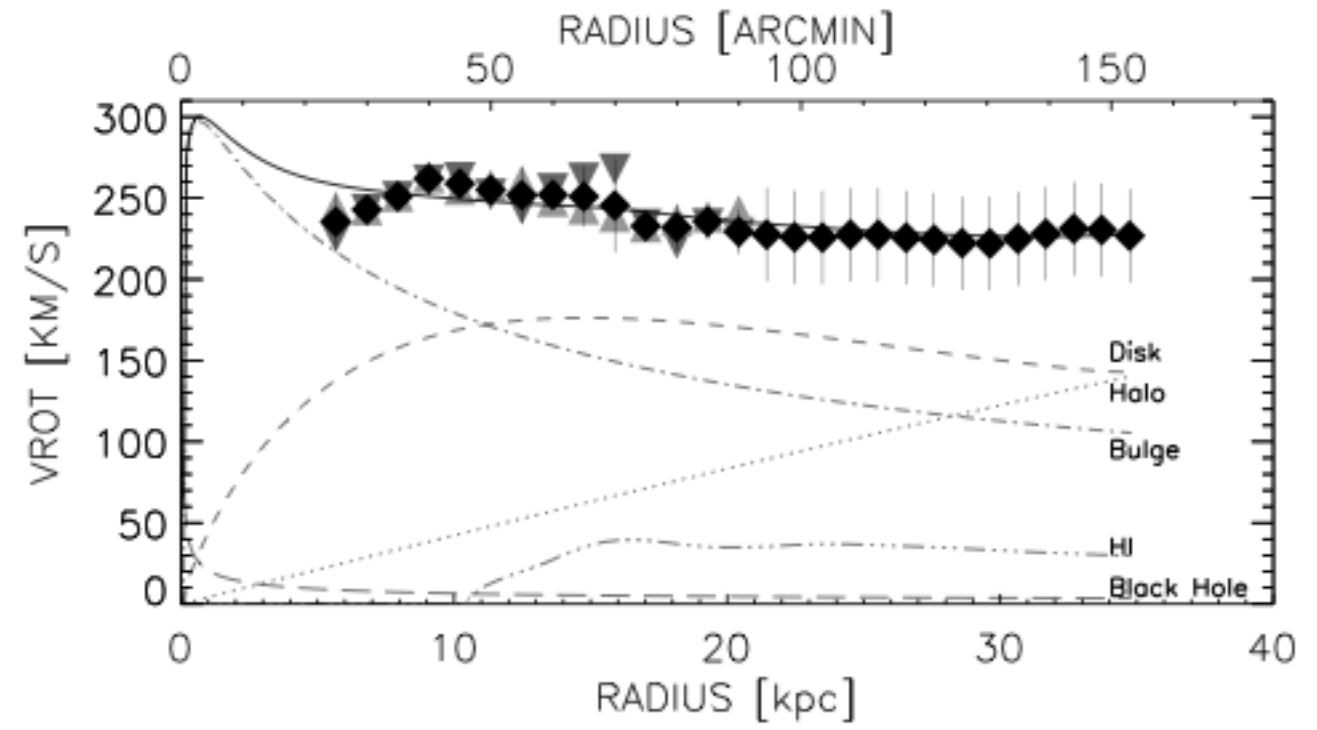


FIG. 2.— Rotation curve and mass model for M31. The new rotation velocities from the Effelsberg and GBT 100-m observations are for $R > 21$ kpc. The velocities for $R \leq 21$ kpc are recomputed from the Unwin (1983) HI data. The upper pointing triangles (light grey) are for the receding side and the bottom pointing (dark grey) ones for the approaching side, as obtained from a tilted-ring model (see text). The solid line is the best fit to the data. Each mass component is identified. A mass of $1.0 \times 10^8 M_\odot$ is used for the central black hole (Bender et al. 2005).

EXTENDED HI ROTATION CURVE AND MASS DISTRIBUTION OF M31

The Astrophysical Journal, 641:L109-L112, 2006 Carignan et al

M31

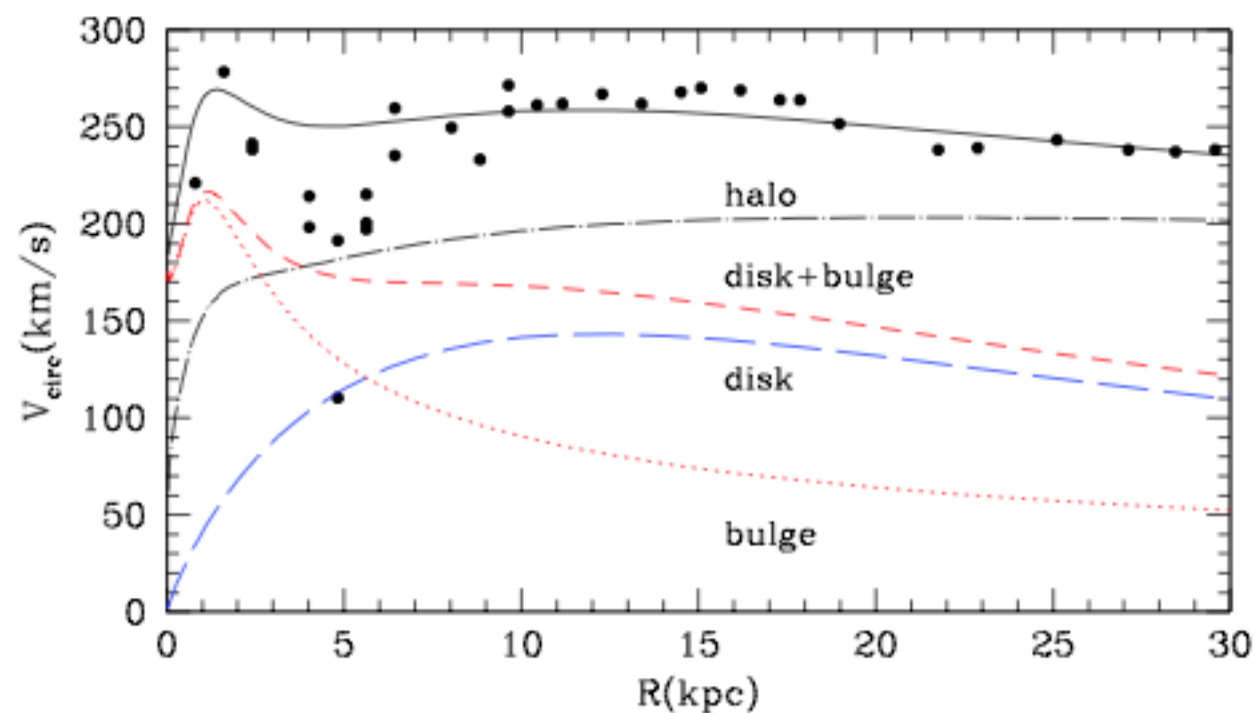


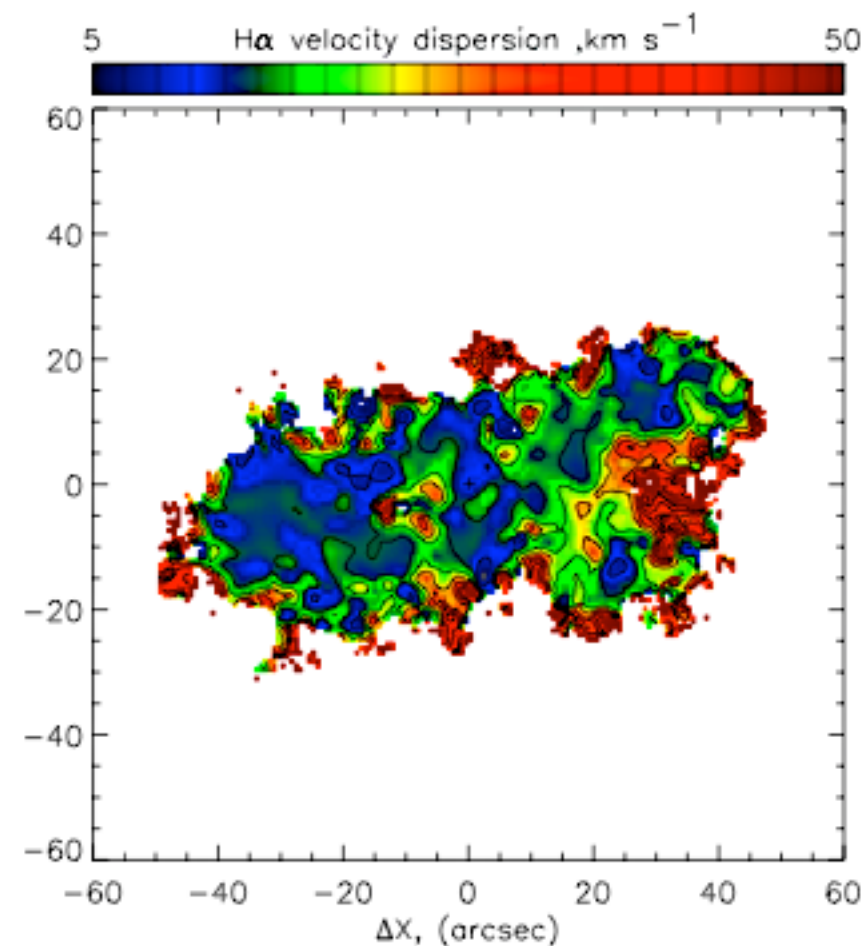
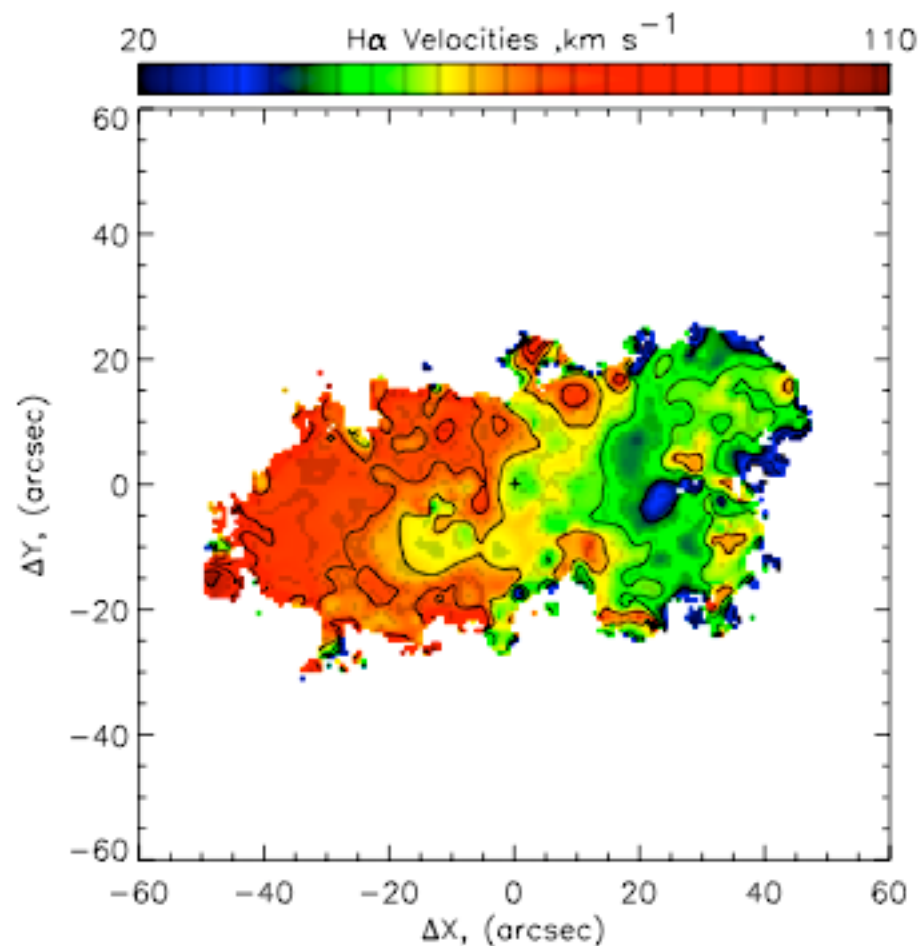
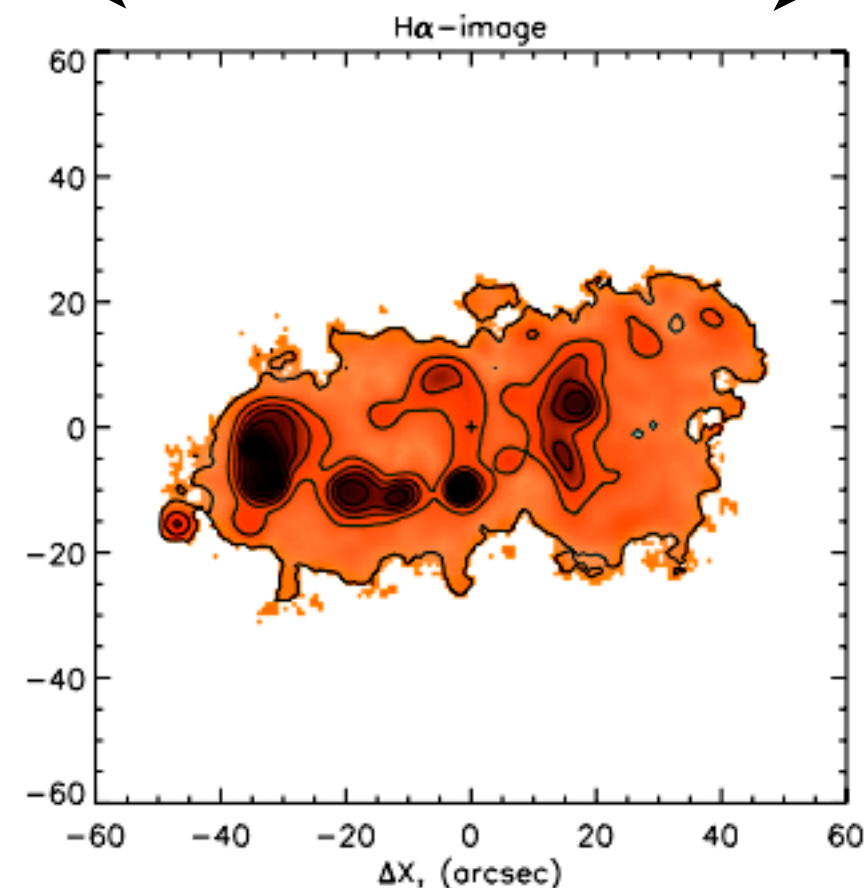
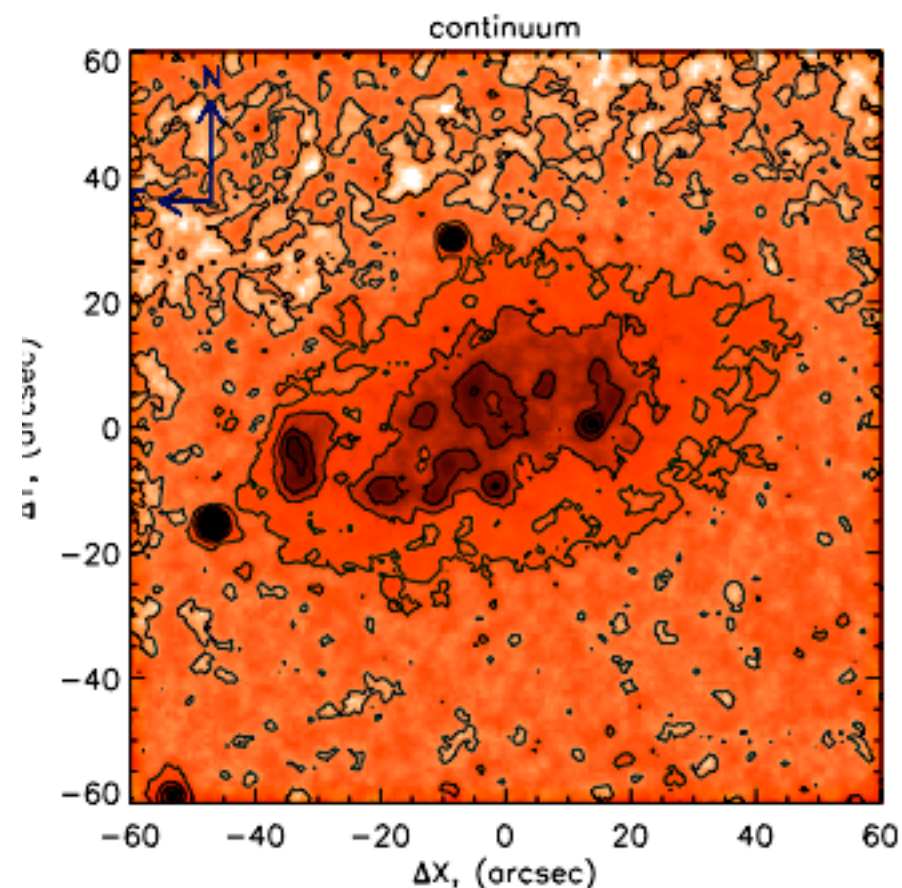
Fig. 4.— Mass distribution (*top panel*) and rotation velocity (*bottom panel*) of the M31 galaxy for Model C_1 . The large dots with error bars are observational

Example:
UGC8508
Distance 2.5 Mpc
 $M_B = -12.9$

Russian 6m
telescope

UGC 8508 6m IFP data (smoothed to 3")

1 kpc



Galaxy, which should not exist:

Cam B (Begum et al 2003)

$$V_{\text{rot+rms}} = 10 \text{ km/s}$$

$$M_B = -12.3$$

$$D = 3.5 \text{ Mpc}$$

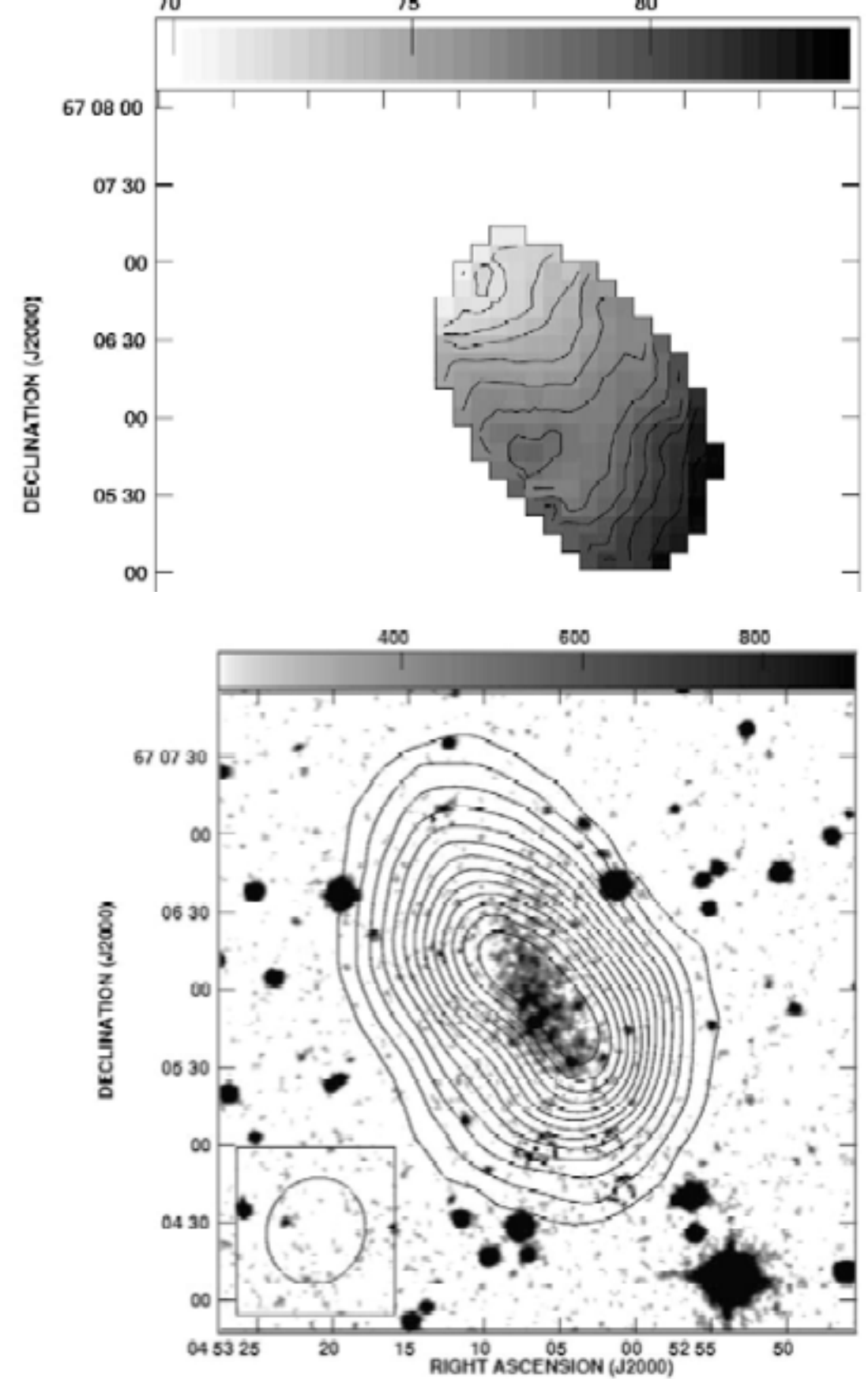
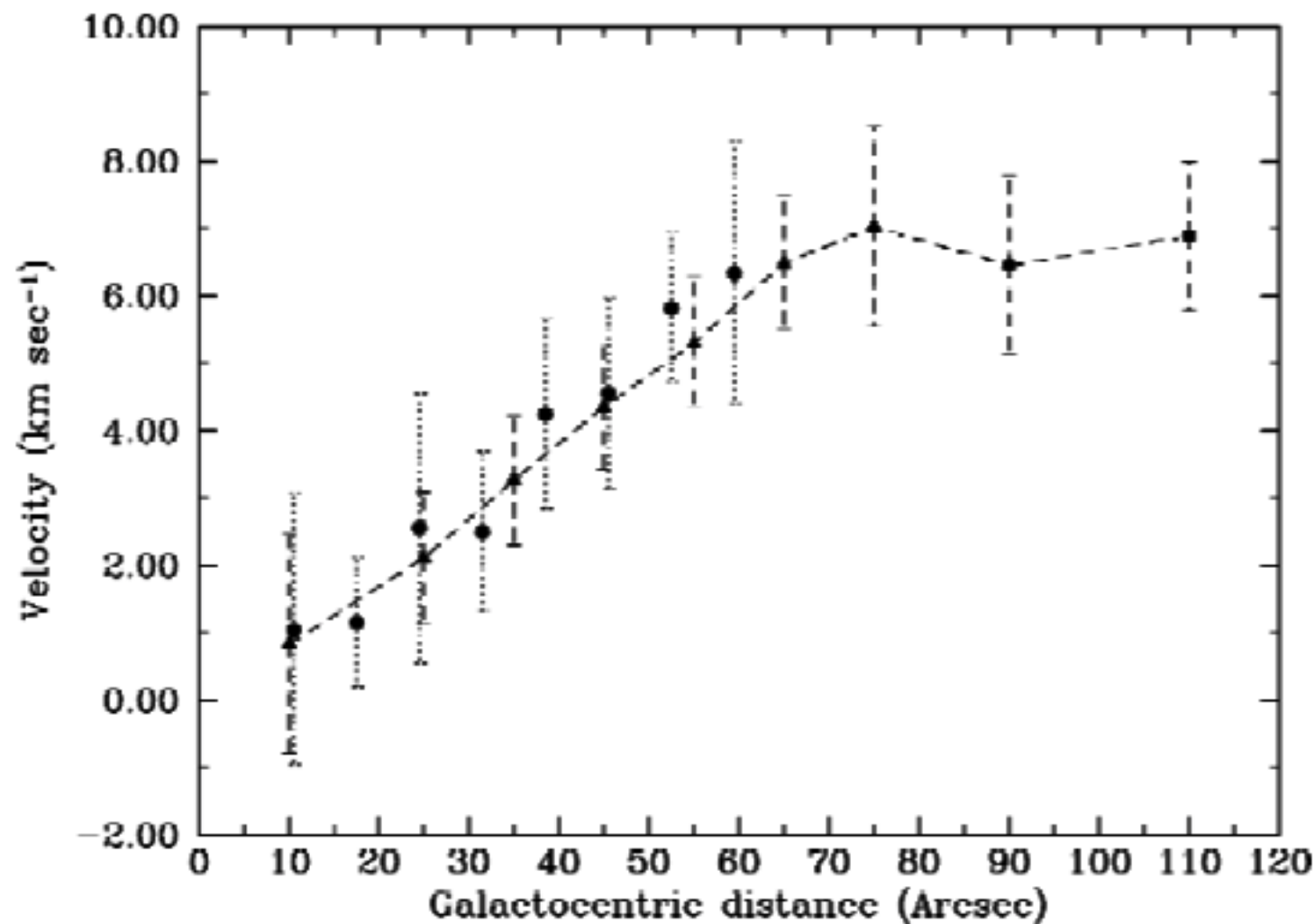


Fig. 3. The digitized Palomar Sky Survey image of Cam B with the GMRT 40'' \times 38'' resolution integrated HI emission (moment 0) map overlaid. The contour levels are 3.7, 8.8, 19.1, 24.3, 29.4, 34.6, 39.8, 44.9, 50.1, 55.2, 60.4, 65.5 and 70.7 $\times 10^{19}$ atoms cm^{-2} .

Structure and kinematics of the nearby dwarf galaxy UGCA 105

Schmidt P. etal A&A 561,A28 (2014)

Absolute <i>B</i> -band magnitude (mag)	M_B	-14.68	(†)
Absolute <i>I</i> -band magnitude (mag)	M_I	-17.80	(†)
Total H I flux (Jy km s^{-1})	$F_{\text{H I}}$	225 ± 11	(1)
H I mass ($10^9 M_\odot$)	$M_{\text{H I}}$	0.64 ± 0.03	(1)
<i>B</i> -band optical radius (″)	r_{25}	169 ± 12	(4)
H I radius (″)	$r_{\text{H I}}$	476 ± 14	(1)
<i>B</i> -band optical radius (kpc)	R_{25}	2.9 ± 0.7	(1)
H I radius (kpc)	$R_{\text{H I}}$	8.0 ± 1.1	(1)

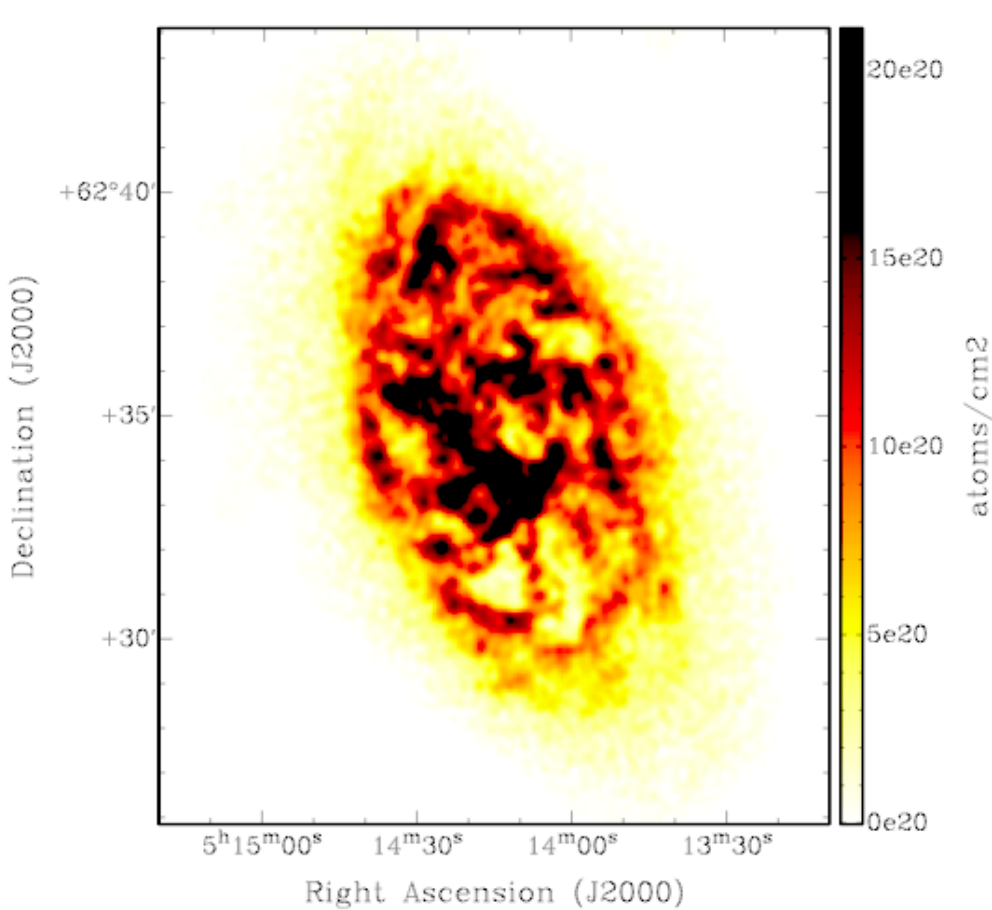


Fig. 3. H I column density distribution of UGCA 105 at $14''.84 \times 13''.14$ (corresponds to 1.01 kpc).

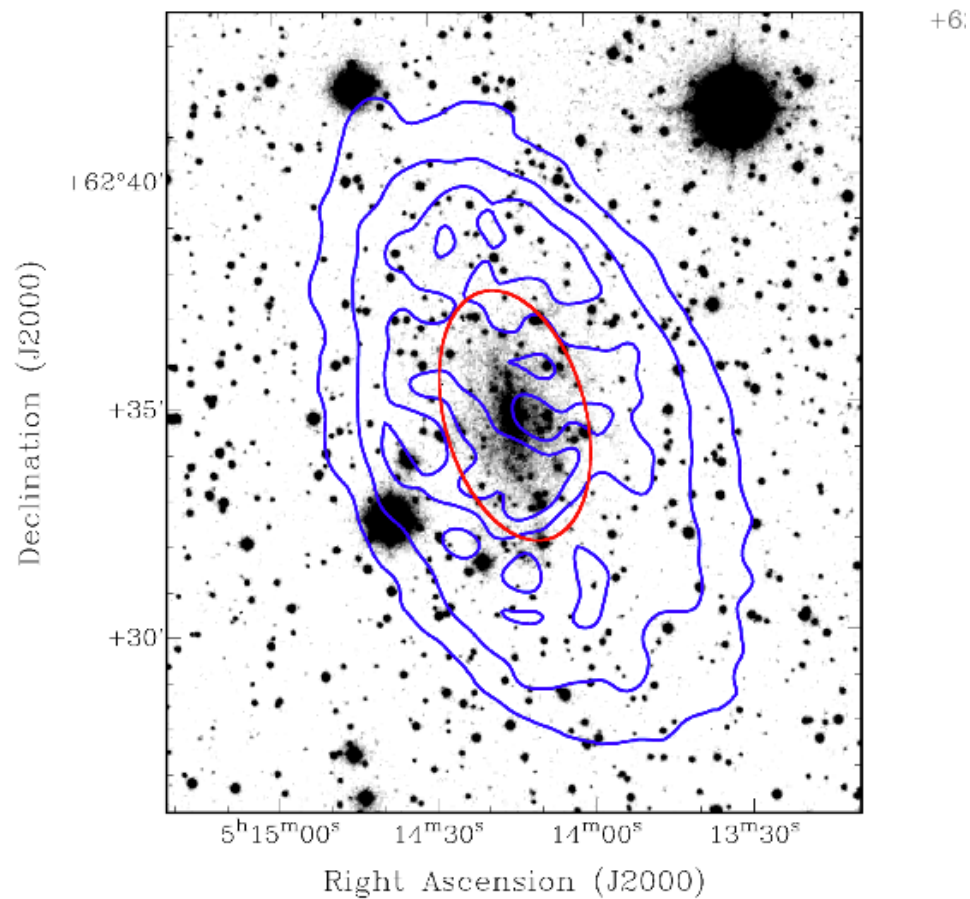


Fig. 4. Left: DSS *I*-band image of UGCA 105, overlaid with contours of the $15 \times 10^{20} \text{ atoms cm}^{-2}$. The red ellipse represents the extent of the optical disk (

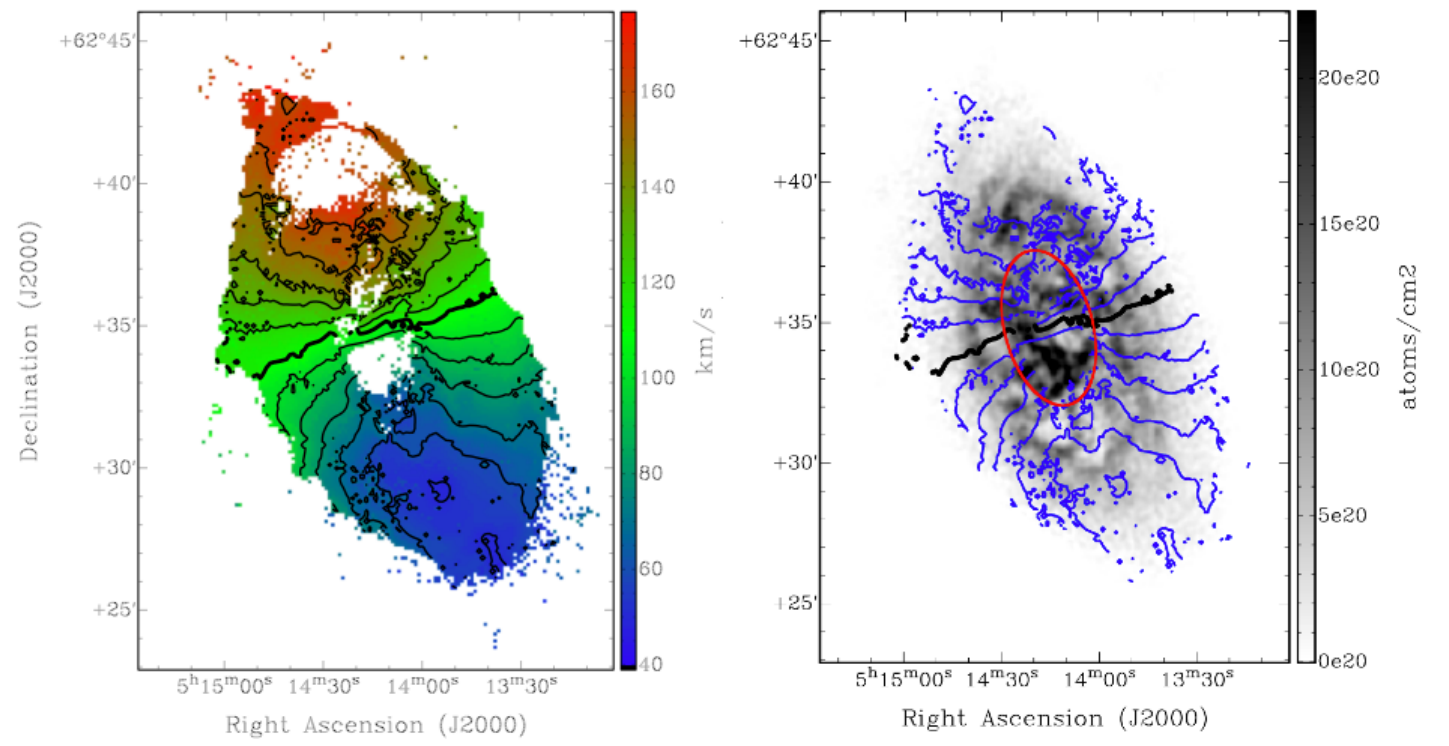
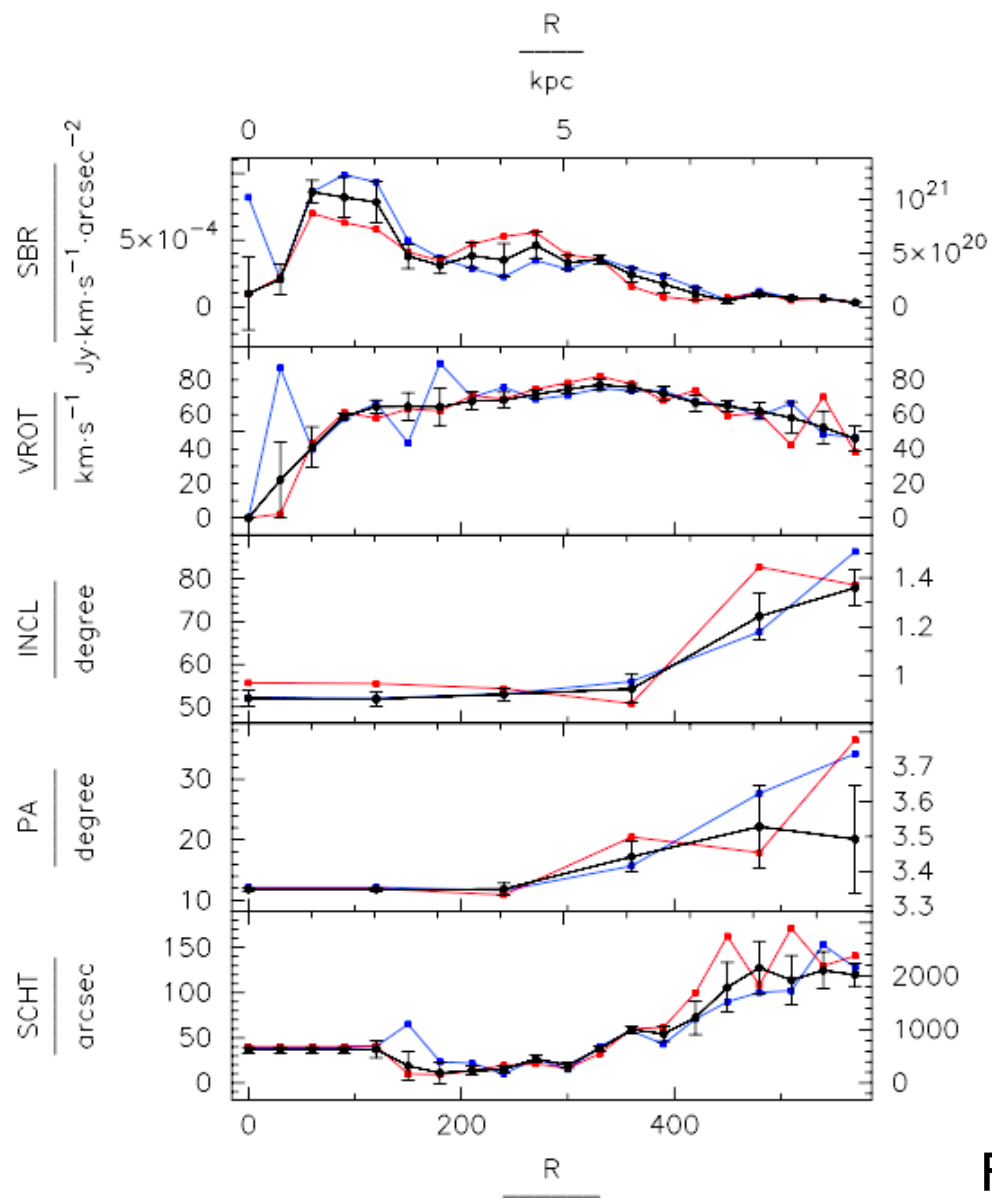
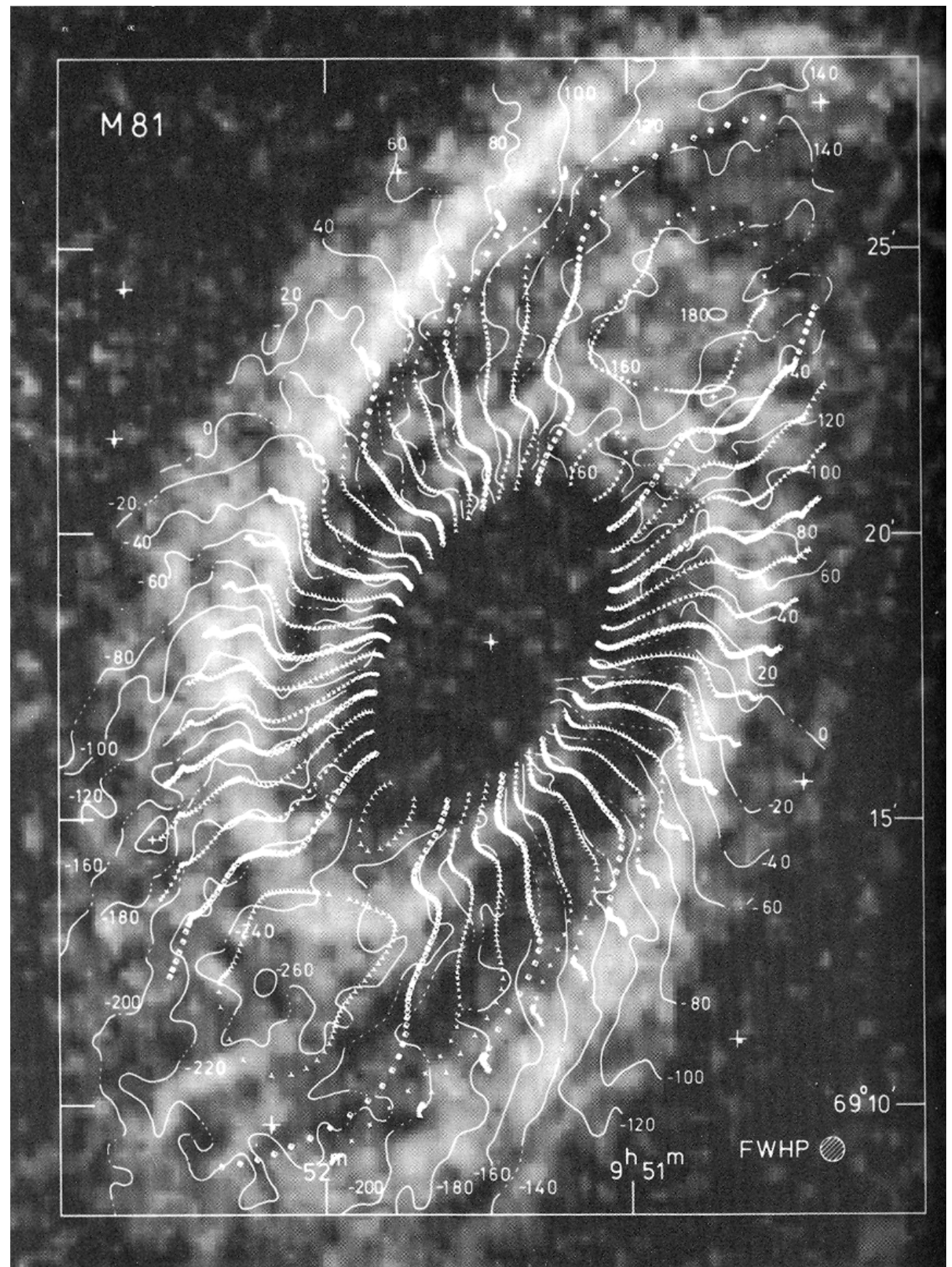


Fig. 5. *Left:* bulk-motion velocity field of UGCA 105, derived from the low-resolution data cube, with contour levels ranging from 50 to 170 km s^{-1} , in steps of 10 km s^{-1} . The thick line represents the systemic velocity of 111 km s^{-1} . *Right:* full-resolution H I column density map, overlaid with velocity contours as shown in the left-hand panel. The red ellipse shows the extent of the optical disk (r_{25}).

Fit parameters are the surface brightness or -density (SBR/SD), rotation velocity (VROT), inclination (INCL), position angle (PA), and scale height (SCHT). Black dots and lines represent the fit to the entire velocity field or data cube, while the blue (red) squares and lines denote the solution for the case in which only the approaching (receding) side was fitted.

Spider diagram of
M81 shows
gravitation effect of
spiral arms



Warps

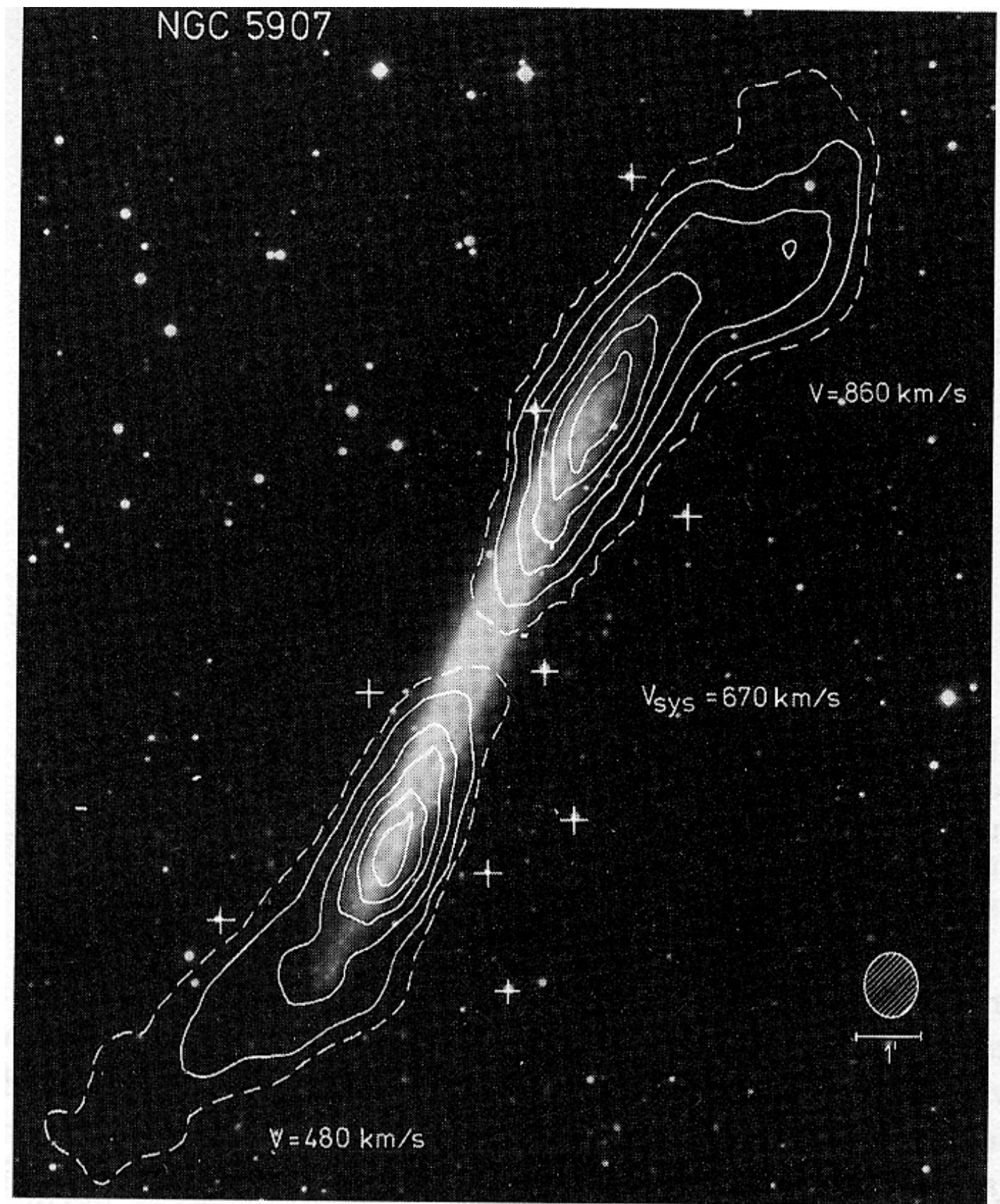
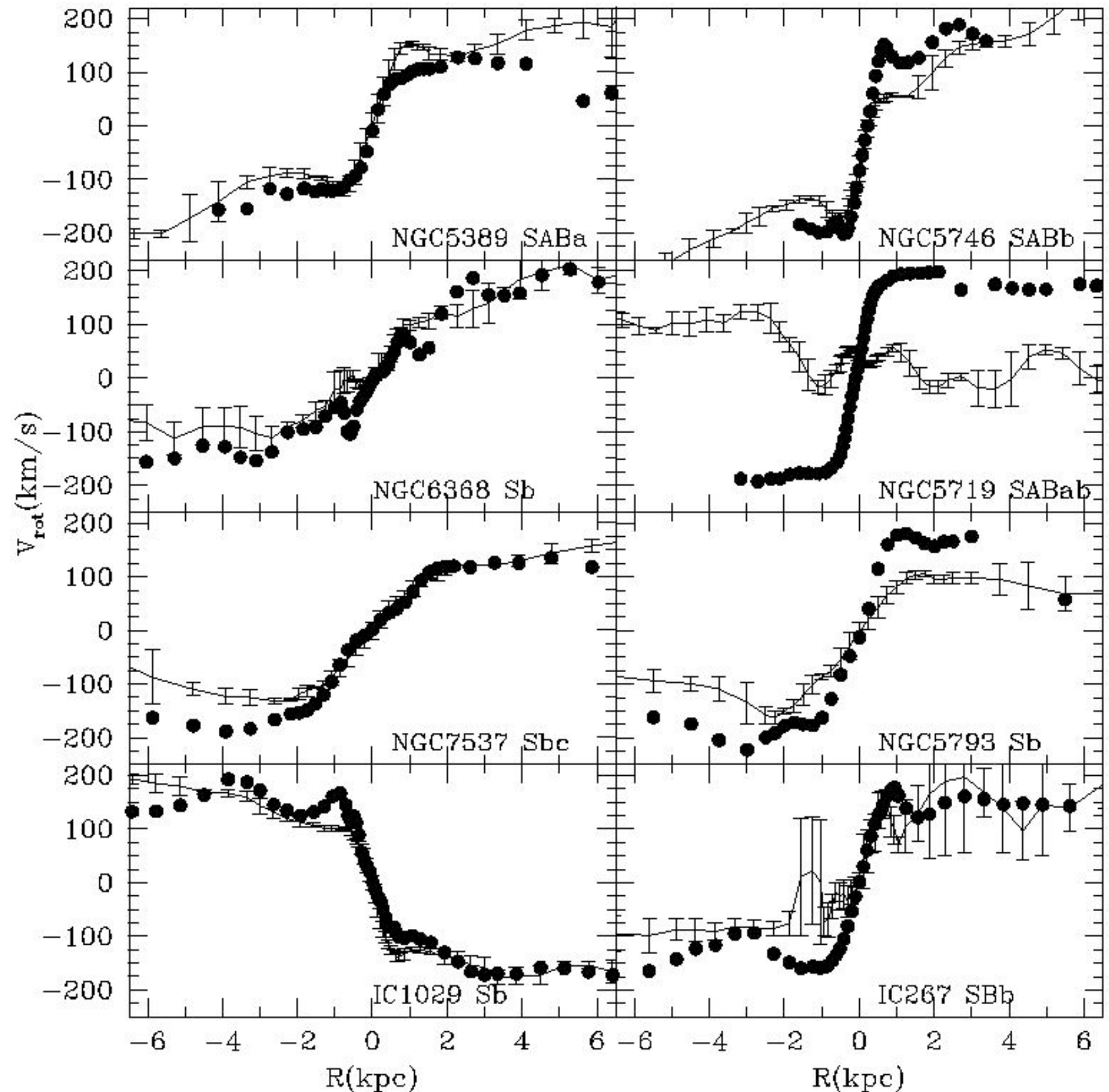


Figure 8.30 The warped neutral hydrogen disk of the nearly edge-on galaxy NGC 5907. Emission by gas that is moving near the systemic velocity of the galaxy has been suppressed for clarity. NGC 5907 has no nearby neighbors that could have recently disturbed it tidally. [After Sancisi (1976) courtesy of R. Sancisi]

Rotation of stars and gas.

Stars rotate slower, but the difference is small (asymmetric drift)

In some cases stars and gas counter rotate.



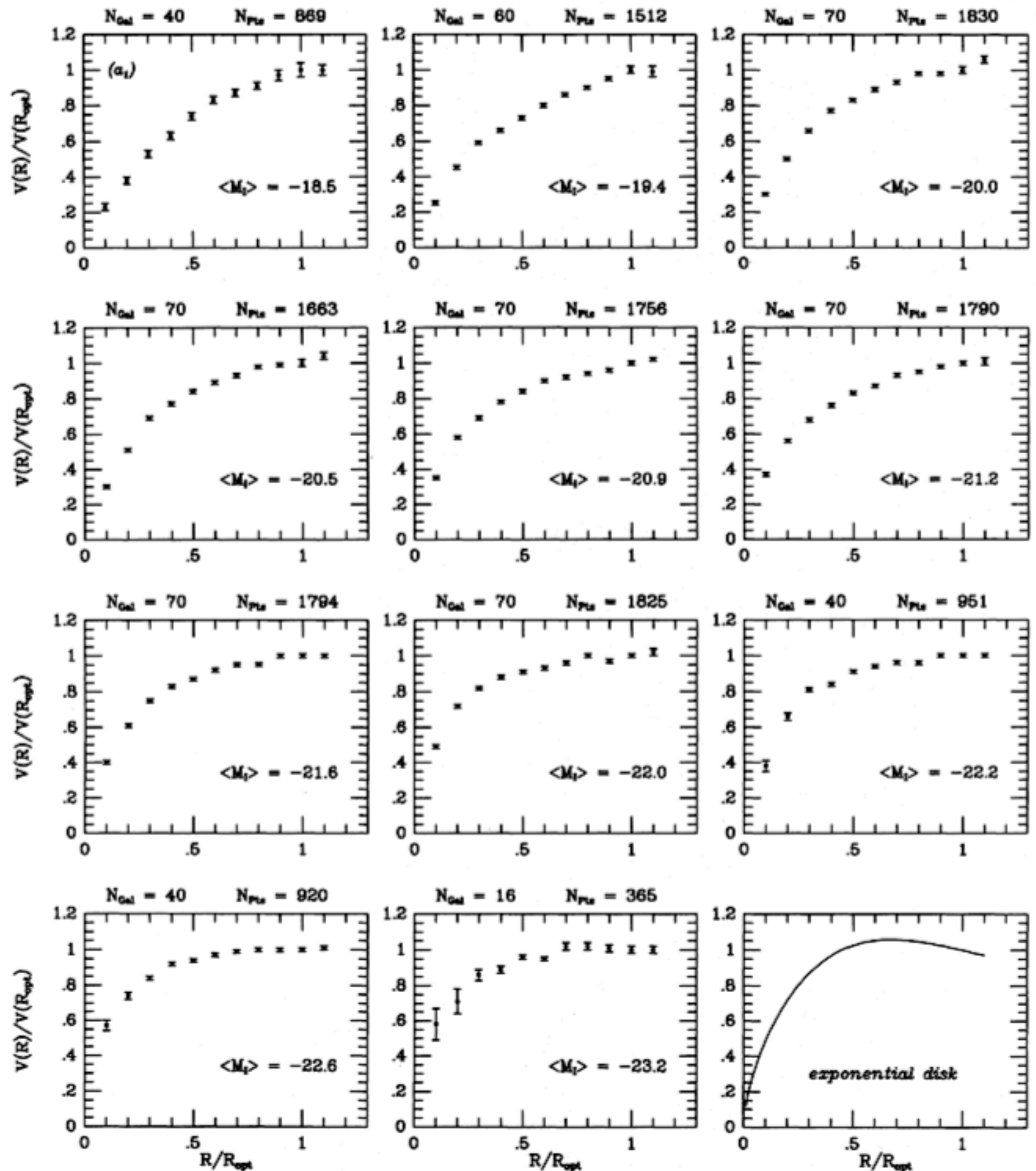
Persic & Salucci (1996)

Properties of rotation curves.

Wide range abs. magnitudes .
Galaxies are supposed to be
either “bulgless” or late type
spirals.

Every rotation curve was
normalized to optical radius
 R_{opt} - radius containing 83%
of the total light. For exp.
disk $R_{\text{opt}} = 3.2R_d$

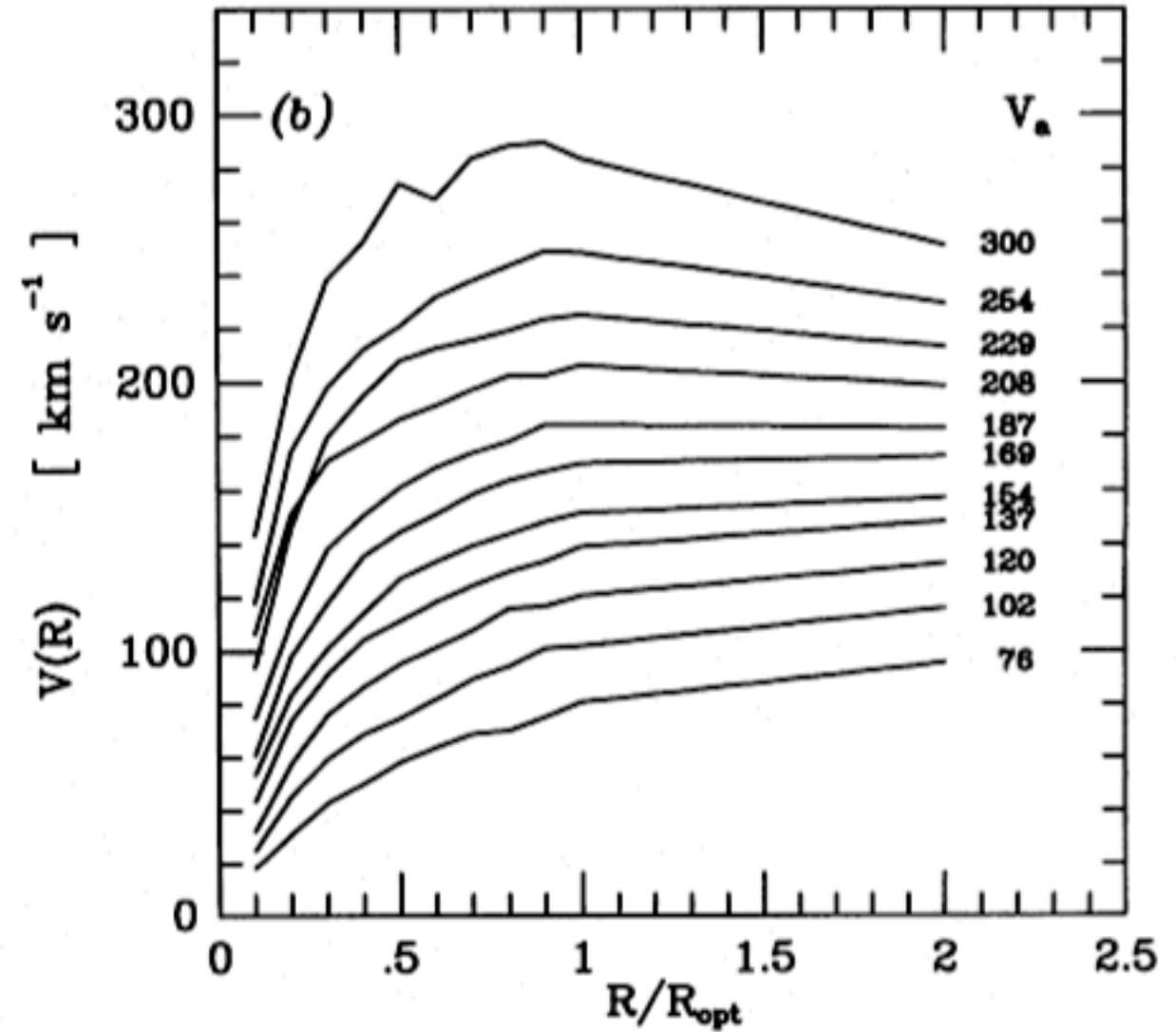
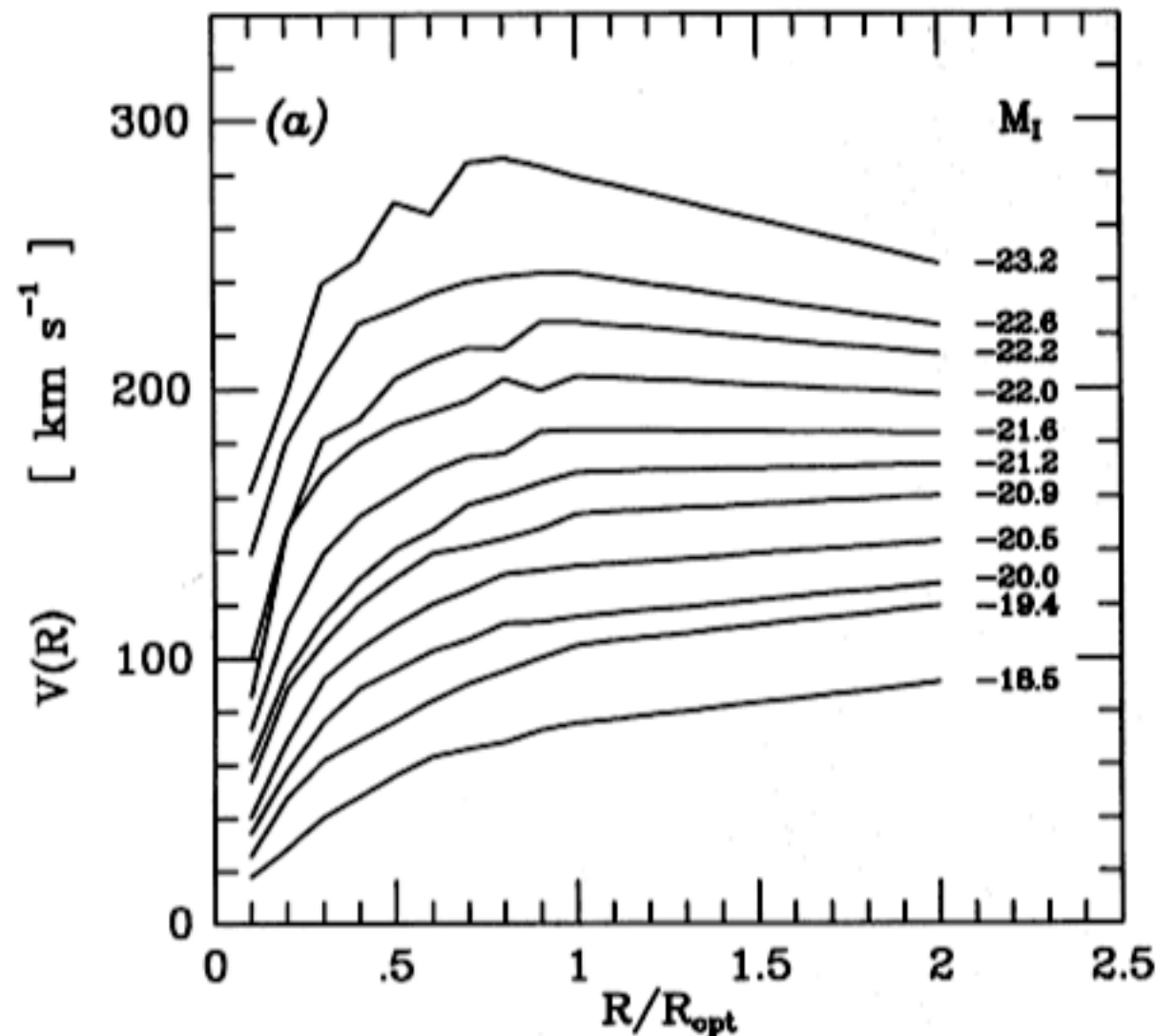
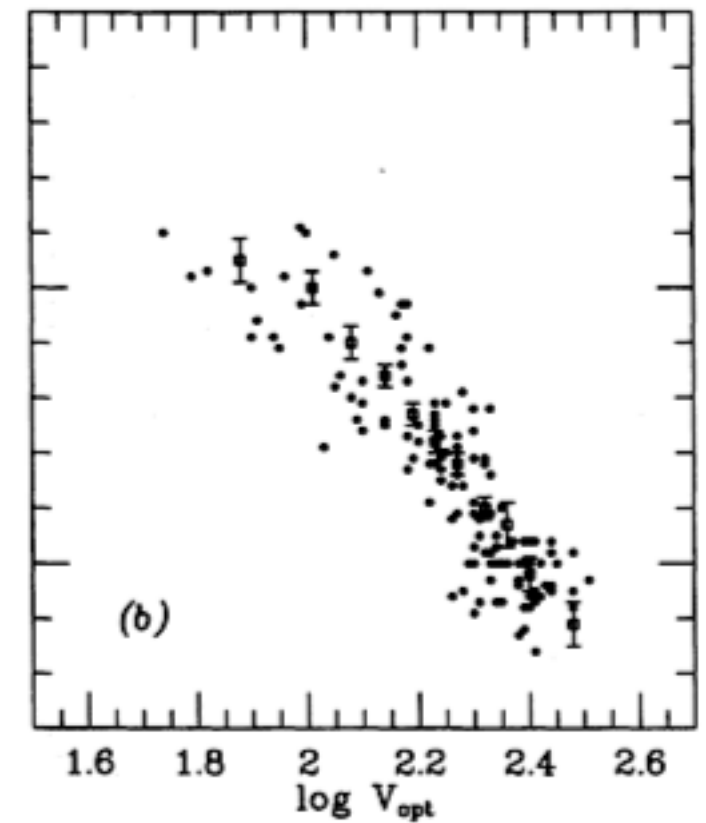
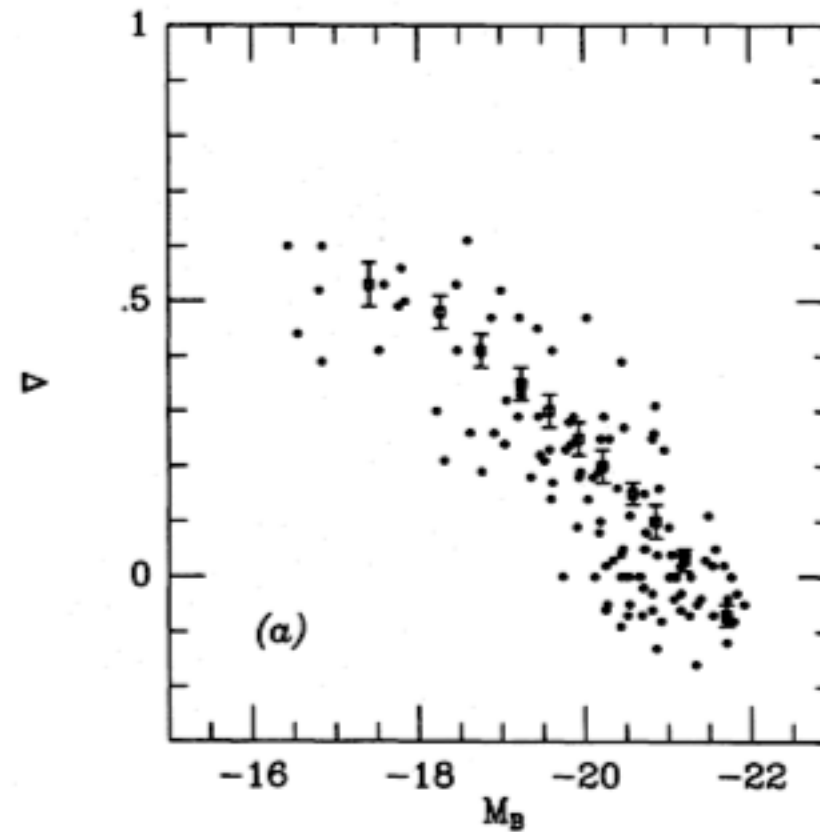
Average rotation curve
depends on abs.magnitude of
galaxy.



Slope of the rotation curve as the function of abs. magnitude

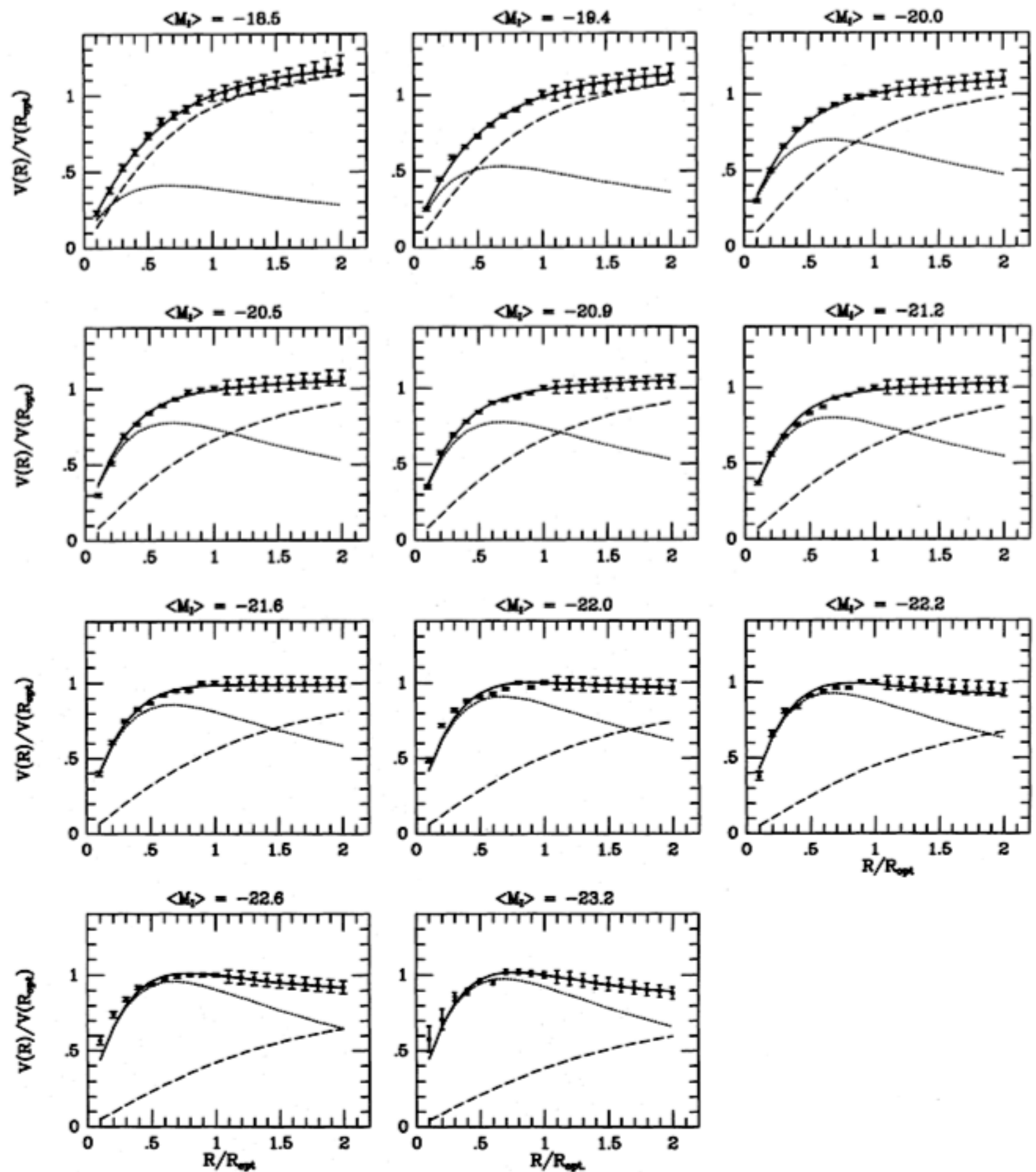
Slope is estimated at R_{opt}

$$\nabla_{\text{lum}} = \left. \frac{d \log V_{\text{lum}}(R)}{d \log R} \right|_{R_{\text{opt}}}$$



Two-component fits. Maximum disk decomposition.

General trend: dwarfs are more DM dominated than giants.



Tendencies:

- ◆ Galaxies with larger L have larger V_{\max}
- ◆ Galaxies with larger L have shorter (in relative units) radii of solid-body (or rising V) rotation
- ◆ Earlier Hubble-type galaxies rotate faster for the same L
- ◆ Fraction of DM inside optical radius increases with decreasing V_{\max}
- ◆ DM is less concentrated than the luminous matter

Mass models

Exponential thin disk: maximum
or sub-maximum disk

DM is spherical:

NFW

$$\rho = \frac{\rho_0}{x(1+x)^2}, \quad x \equiv \frac{r}{r_s}$$

Nuker

$$\rho = \frac{\rho_0}{\left(\frac{r}{r_0}\right)^\gamma \left[1 + \left(\frac{r}{r_0}\right)^\alpha\right]^{\frac{(\beta-\gamma)}{\alpha}}}$$

Burkert

$$\rho = \frac{\rho_0}{\left(1 + \frac{r}{r_b}\right) \left(1 + \left(\frac{r}{r_b}\right)^2\right)}$$

Example of rotation curve a low surface brightness galaxy.

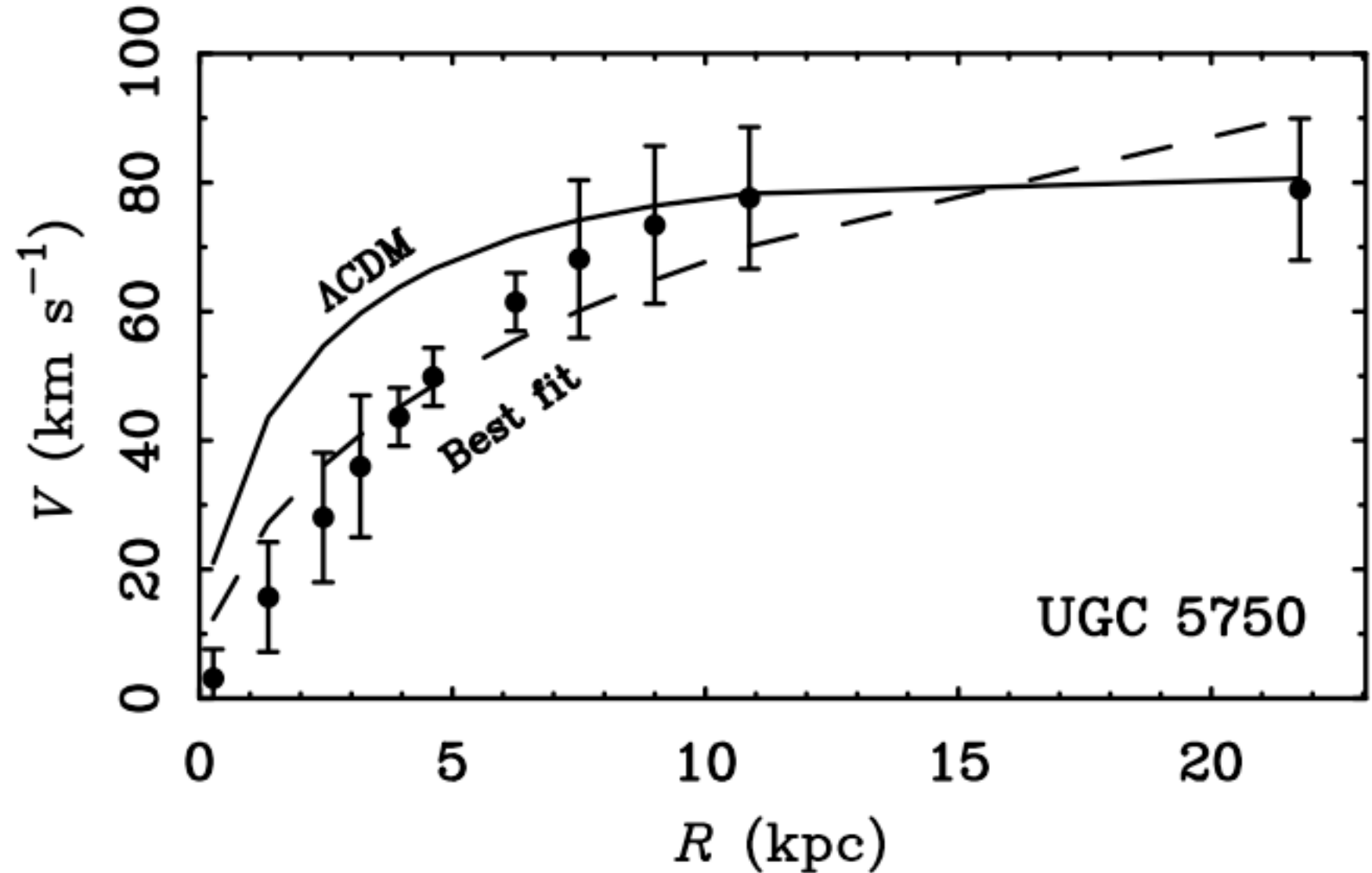


Fig. 1.— The rotation curve of the low surface brightness galaxy UGC 5750. Also shown are the best fitting NFW halo parameters ($c = 2.6$, $V_{200} = 123 \text{ km s}^{-1}$; dashed line) for the limiting case of a zero mass (minimum) disk, and what the NFW halo should look like for a galaxy of this rotation velocity in the standard ΛCDM cosmology ($c = 10$, $V_{200} = 67 \text{ km s}^{-1}$; solid line). The excess of the solid line over the data illustrates the cuspy halo problem. Though an NFW fit can be made (dashed line), it is a poor description of the data, and requires a very low concentration ($c = 2.6$ does not occur in any plausible cosmology). These problems become more severe as allowance is made for stars (BMR; BB).

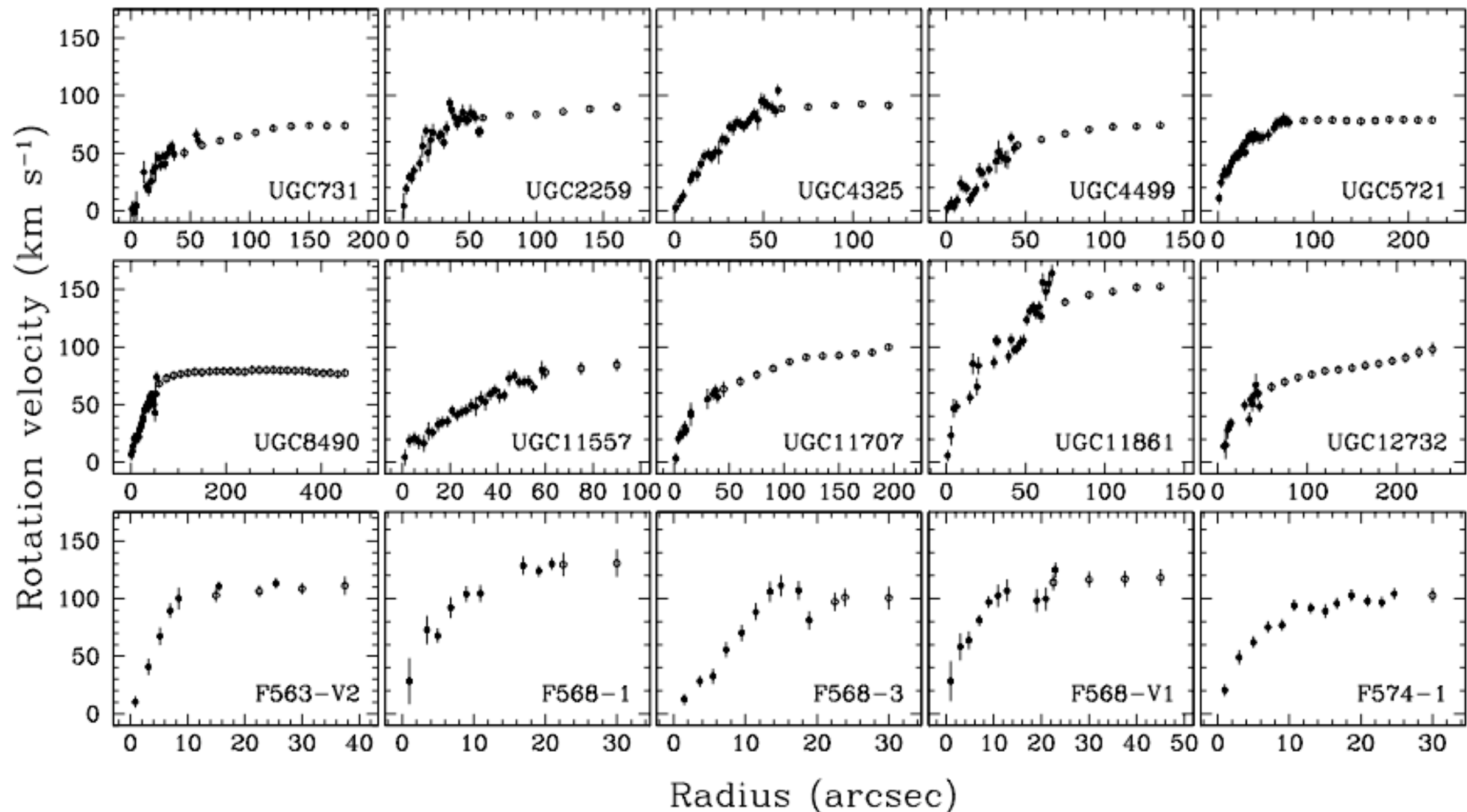


FIG. 2.— Combined H α /H I rotation curves. The filled circles represent the H α rotation curves as derived in this paper, the open circles are the H I rotation curves from Swaters (1999) for the dwarf galaxies and from de Blok et al. (1996) for the LSB galaxies.

DDO 39

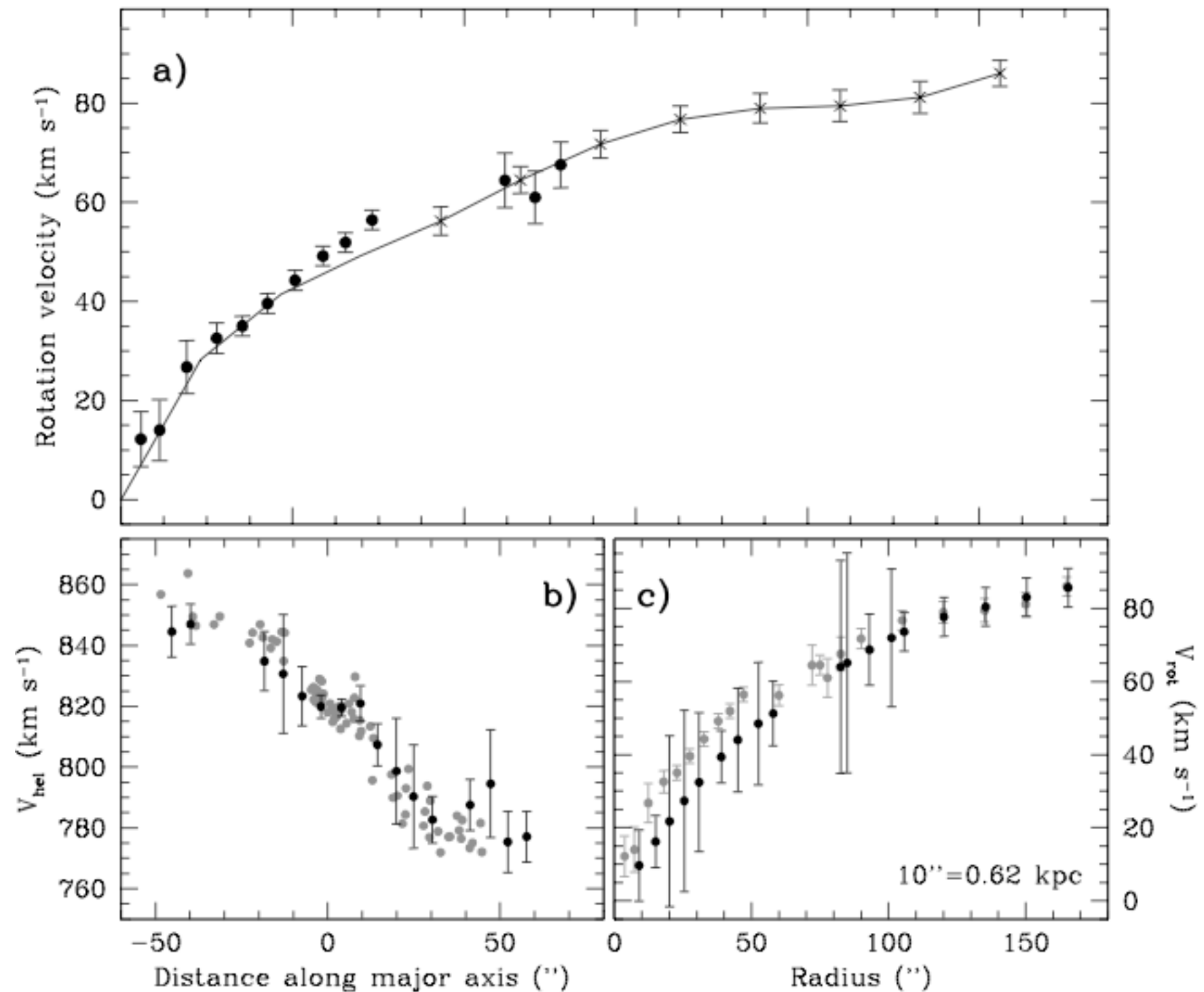


FIG. 2.— **a)** Hybrid rotation curve from SparsePak data (*dots*) and the HI data from S99 (*crosses*). The rotation curve from S99 is given by the solid line. **b)** Comparison of dBB's data (*black dots*) to SparsePak data within 2.5" of the major axis (*grey dots*). **c)** Comparison of dBB's and our rotation curve, coding as in panel b.

THE KINEMATICS IN THE CORE OF THE LOW SURFACE BRIGHTNESS GALAXY DDO 39

R. A. SWATERS^{1,2}, M. A. W. VERHEIJEN^{3,4}, M. A. BERSHADY³, D. R. ANDERSEN⁵
The Astrophysical Journal, draft version March 5, 2003

ABSTRACT

We present a high resolution, SparsePak two-dimensional velocity field for the center of the low surface brightness (LSB) galaxy DDO 39. These data are a significant improvement on previous HI or H α long slit data, yet the inner rotation curve is still uncertain due to significant noncircular and random motions. These intrinsic uncertainties, probably present in other LSB galaxies too, result in a wide range of inner slopes being consistent with the data, including those expected in cold dark matter (CDM) simulations. The halo concentration parameter provides a more useful test of cosmological models than the inner slope as it is more tightly constrained by observations. DDO 39's concentration parameter is consistent with, but on the low end of the distribution predicted by CDM.

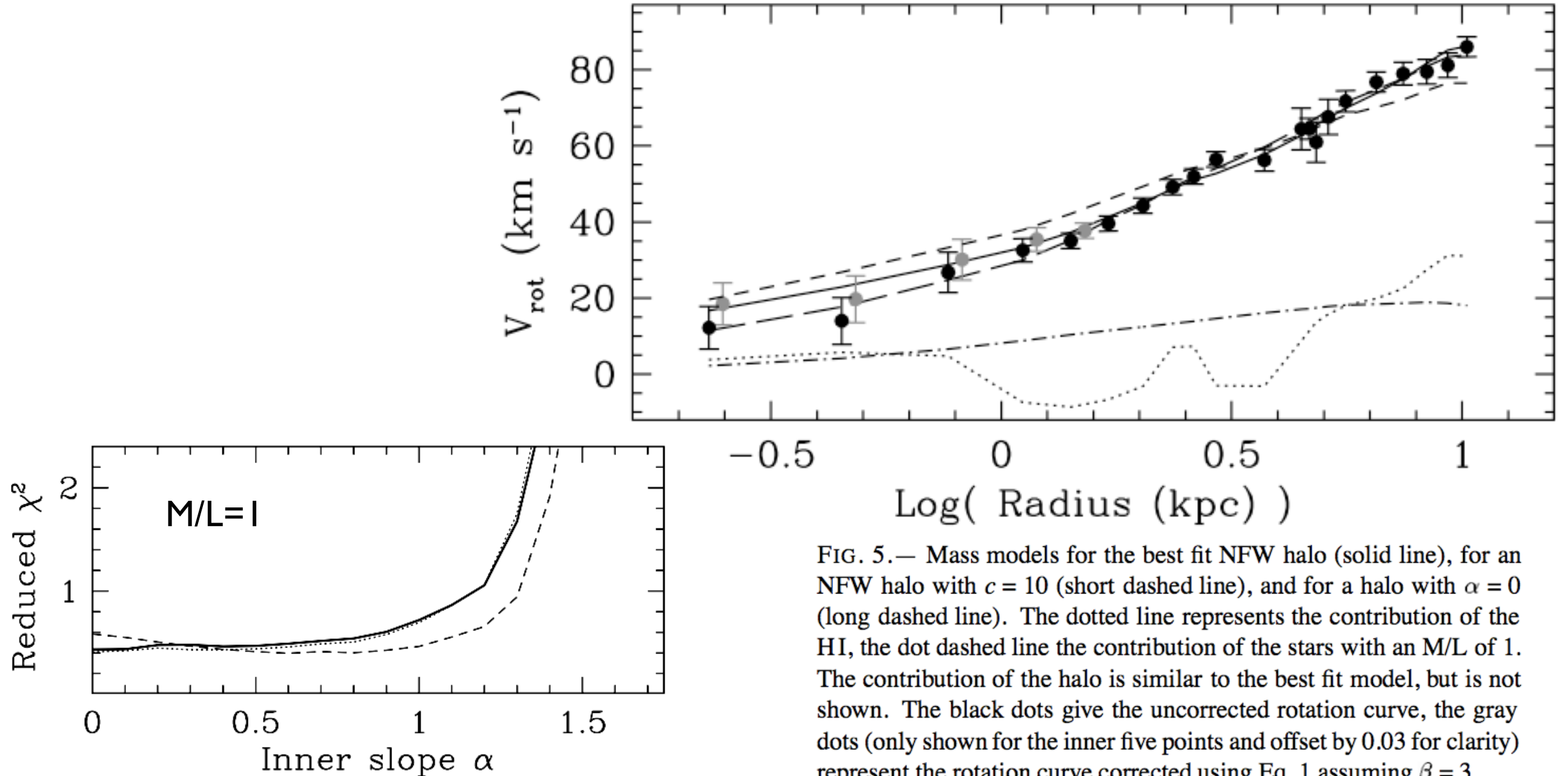
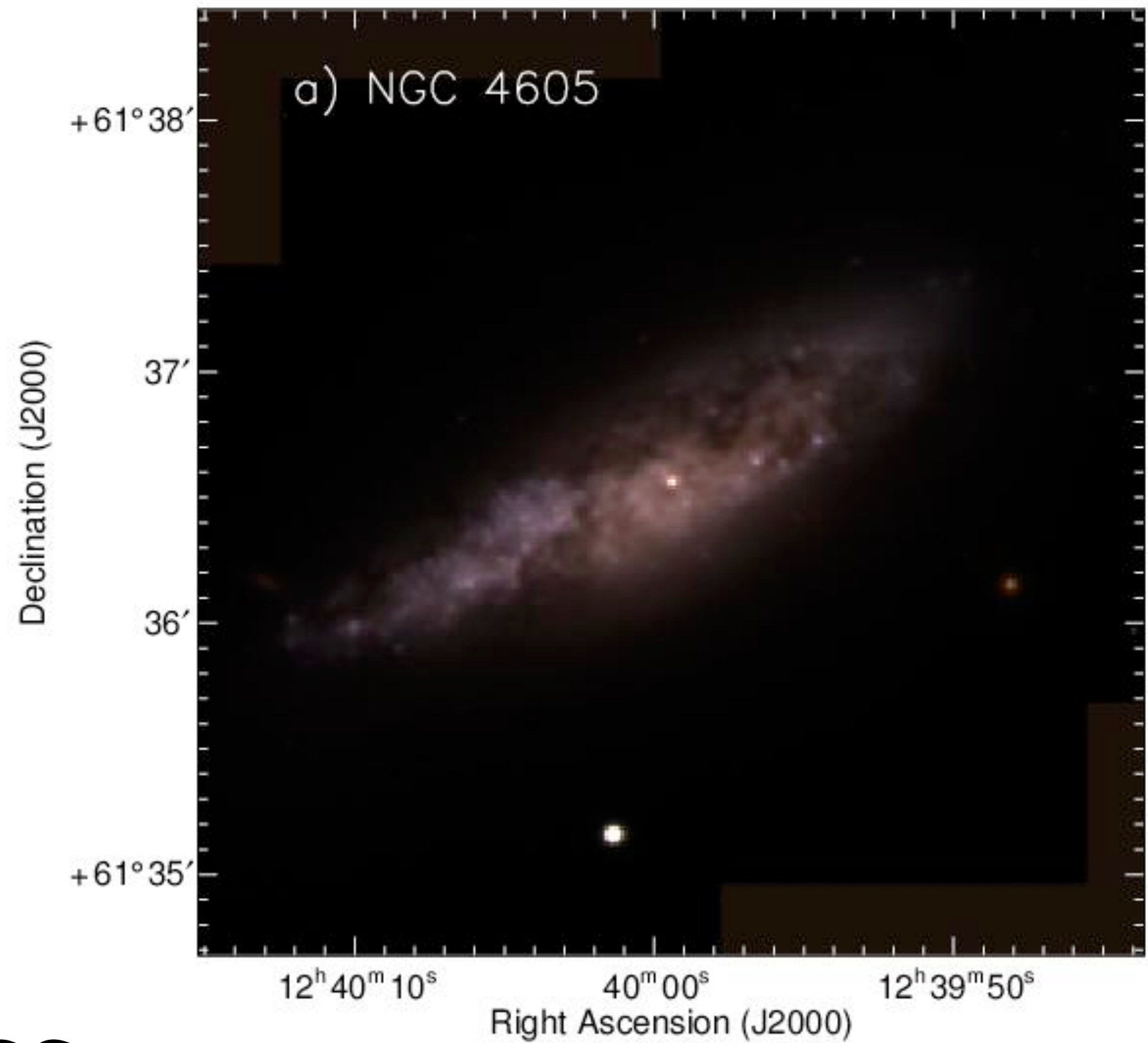
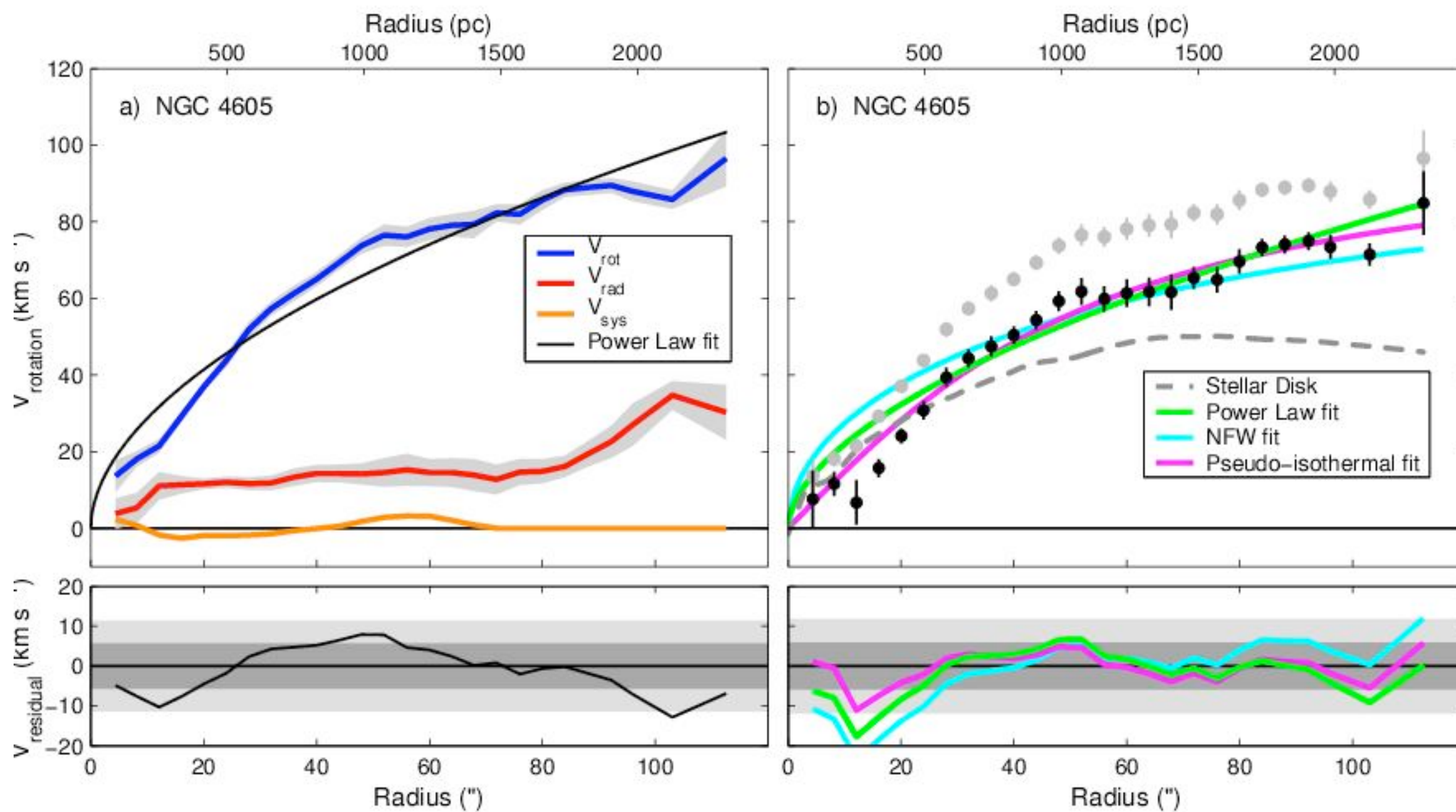


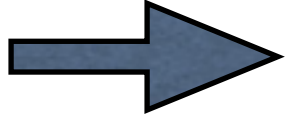
FIG. 5.— Mass models for the best fit NFW halo (solid line), for an NFW halo with $c = 10$ (short dashed line), and for a halo with $\alpha = 0$ (long dashed line). The dotted line represents the contribution of the HI, the dot dashed line the contribution of the stars with an M/L of 1. The contribution of the halo is similar to the best fit model, but is not shown. The black dots give the uncorrected rotation curve, the gray dots (only shown for the inner five points and offset by 0.03 for clarity) represent the rotation curve corrected using Eq. 1 assuming $\beta = 3$.



Dwarf galaxy NGC
4605: radial motions?



Two ways of recovering distribution of the mass

Assume models  get parameters

Invert rotation curve

$$-F_r = \frac{d\Phi}{dr} = \frac{v_c^2}{r}, \quad (1)$$

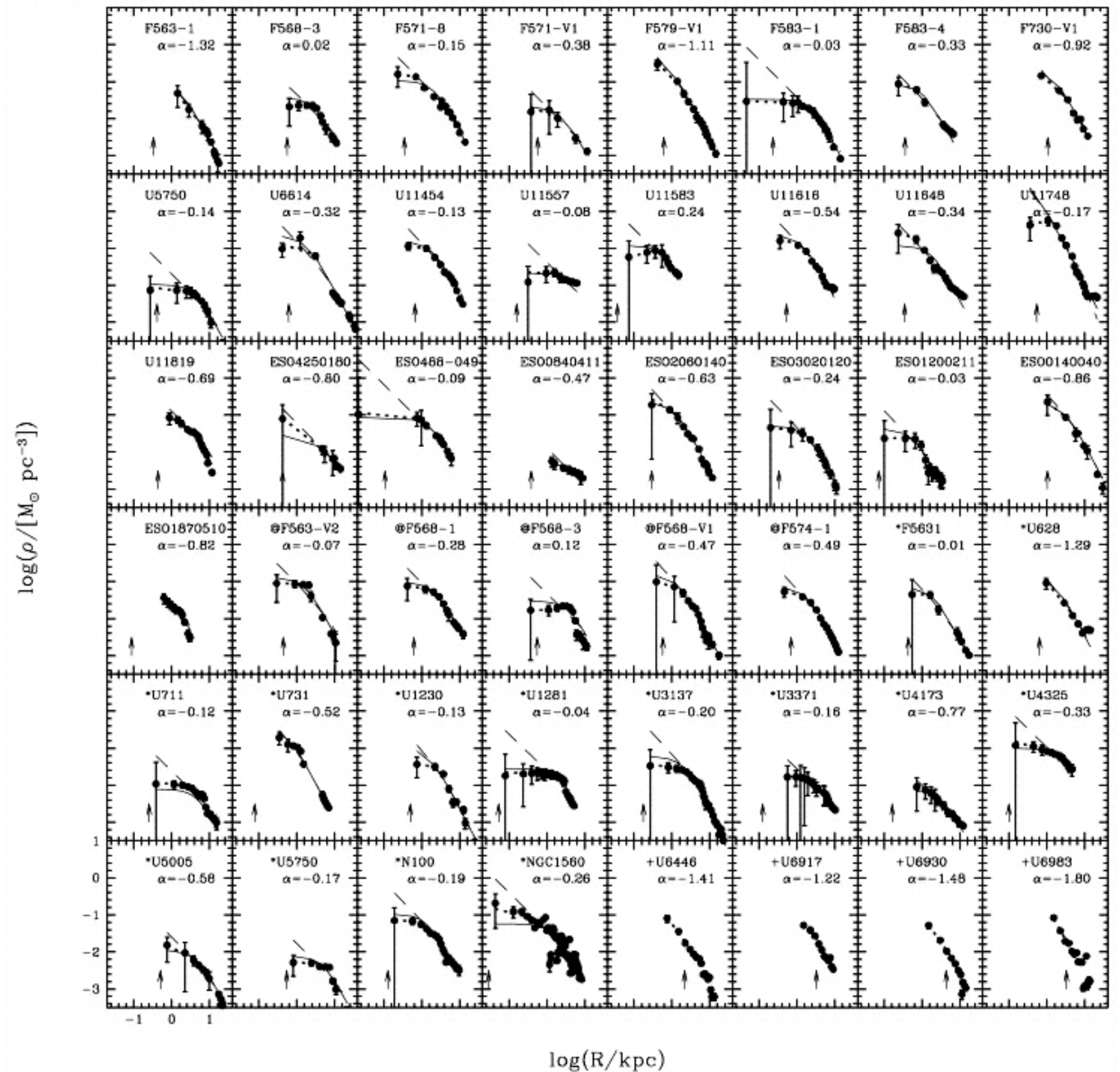
where F_r is the radial force, Φ the gravitational potential, r the galactocentric radius and v_c the circular velocity. The total gravitational potential is the sum of the gravitational potentials of the individual mass components in a galaxy. Here, we assume that the galaxy consists of three main components: a stellar disk, a gaseous disk, and a spherical dark halo. Its total circular velocity is then given by:

$$v_c = \sqrt{\Upsilon_* v_d^2 + \eta v_{\text{HI}}^2 + v_h(p_1, \dots, p_n)^2}, \quad (2)$$

where Υ_* is the stellar mass-to-light ratio, v_d is the rotation curve of the stellar disk for a stellar mass-to-light ratio of unity, η represents the inclusion of the contribution of helium to the gaseous component, assumed to be 1.32, v_{HI} is the rotation curve of the HI only, and $v_h(p_1, \dots, p_n)$ represents the dark halo, where p_1 to p_n are parameters describing its mass distribution. Each of the components in this equation is described in more detail below. The best fitting mass model for a given dark halo model is determined by fitting Eq. 2 to the observed rotation curve, with Υ_* and p_1 to p_n as free parameters.

$$4\pi G\rho(r) = 2 \frac{v}{r} \frac{\partial v}{\partial r} + \left(\frac{v}{r}\right)^2,$$

deBlok et al. 2001



We derive the mass density profiles of dark matter halos that are implied by high spatial resolution rotation curves of low surface brightness galaxies. We find that, at small radii, the mass density distribution is dominated by a nearly constant density core with a core radius of a few kiloparsecs. For $\rho(r) \sim r^{\alpha}$, the distribution of inner slopes α is strongly peaked around $\alpha = -0.2$. This is significantly shallower than the cuspy $\alpha \leq -1$ halos found in cold dark matter simulations. While the observed

Different
conclusions

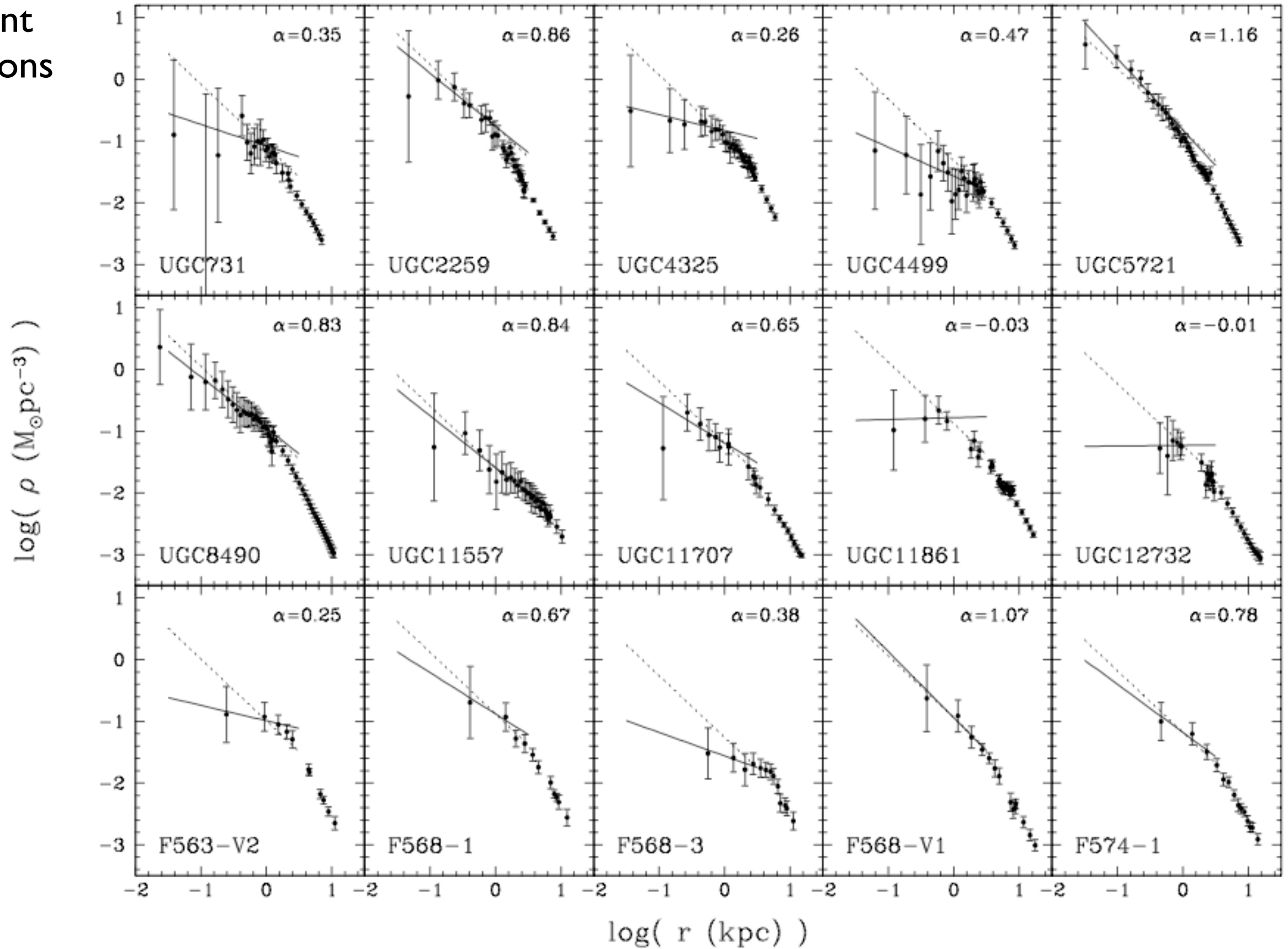


FIG. 5.— Log-log plots of the density distribution as derived by inverting the observed rotation curves, following the procedure as described in Section 5.1. The solid line represents a weighted least-squared fit to the parts of the profile within the break radius, the dotted lines represent a slope of $\alpha = 1$.

